

# The Geometry of Flux Surfaces with Quasi-Poloidal Symmetry

Rishin Madan,<sup>1,2†</sup> Wrick Sengupta,<sup>1</sup> Elizabeth J. Paul,<sup>3</sup>  
 Mohammed Haque,<sup>3</sup> Richard Nies,<sup>4,5</sup> and Amitava Bhattacharjee<sup>1</sup>

<sup>1</sup>Department of Astrophysical Sciences, Princeton University, Princeton, NJ 08543, USA

<sup>2</sup>Princeton Plasma Physics Laboratory, Princeton, NJ 08540, USA

<sup>3</sup>Columbia University, New York, NY 10027, USA

<sup>4</sup>Rudolf Peierls Centre for Theoretical Physics, Parks Road, Oxford, OX1 3PU, UK

<sup>5</sup>New College, Holywell Street, Oxford, OX1 3BN, UK

Quasi-poloidal (QP) magnetic fields have desirable properties for confining plasma: no radial drift of guiding centres (with positive implications for neoclassical transport), zero Pfirsch-Schlüter current, a lower level of damping for poloidal flows, leading to reduced anomalous transport, and possible stability benefits. Despite their attractive properties, QP fields are not amenable to the near-axis expansion, a major theoretical tool for understanding toroidal fields. In this paper, we provide a novel framework for defining and understanding QP flux surfaces. This framework relies on a simplification that transforms the task of finding a quasi-poloidal flux surface from a 3D problem to a 2D problem. This simplification also applies to asymmetric magnetic mirrors with desirable properties. We sketch how this 2D problem can form the basis of an efficient optimisation problem for finding QP flux surfaces. We leverage this 2D problem for theoretical understanding: for instance, we identify one class of QP flux surfaces that are naturally flat mirrors (Velasco *et al.* 2023). The reduced model is validated against numerically optimised QP equilibria. We further utilise the reduced model to explain the prevalence of cusps, high mirror ratios, and narrow pinch points in these numerical equilibria.

## 1. Introduction

The stellarator is a device that confines plasma by generating a toroidal magnetic field, envisaged for the purpose of energy production by controlled fusion (Spitzer 1958). The shaping of the magnetic field critically affects properties of the plasma, such as confinement time and pressure profiles.

We focus on quasi-poloidally symmetric (QP) magnetic fields with negligible enclosed toroidal current. Such fields are a subset of quasisymmetric fields (Nührenberg & Zille 1988; Boozer 1995; Rodríguez *et al.* 2020), which have a symmetry of the magnetic field strength such that the guiding-centre motion of the particles possesses a conserved canonical momentum, analogous to the axisymmetric, tokamak case. Quasisymmetry itself is a special case of *omnigeneity*, for which the bounce-averaged radial drift of the trapped particles vanishes (Hall & McNamara 1975). When omnigenous fields have poloidally closed contours of the magnetic field strength, they are called quasi-isodynamic (QI). Quasi-poloidal symmetry is the particular case of quasisymmetry where the magnetic field strength is constant on poloidal loops, as opposed to toroidal (quasi-axisymmetry) or helical loops (quasi-helical symmetry). QP is thus also a special case of QI.

† Email address for correspondence: rishin.madan@princeton.edu

QP magnetic fields have advantages beyond those of other quasisymmetric and QI configurations. Given that the enclosed toroidal current of a QP flux surface vanishes, which is often a good approximation for stellarators, the field lines are geodesics of the surface. Consequently, the radial drift of guiding centres vanishes pointwise—the ideal scenario for collisionless particle confinement. Hence, there is no radial neoclassical transport to first order in guiding-centre motion. For the same reasons, the bootstrap current vanishes. The Pfirsch-Schlüter current also vanishes, resulting in zero [Shafranov \(1963\)](#) shift and potentially higher beta limits. Furthermore, QP has the potential to reduce anomalous transport. Uniquely, there is a lower level of damping for poloidal flows ([Shaing & Callen 1983](#)). Thus, QP allows for shearing flows that can suppress turbulence ([Wobig 1999; Terry 2000; Spong et al. 2005; Alcusion et al. 2016](#)). As a final advantage of QP, there is evidence that second stability is possible in high-beta, compact, QP fields ([Ware et al. 2004](#)).

There has been recent success in optimising for QI fields with suitable properties for plasma confinement ([Goodman et al. 2023; Sánchez et al. 2023](#)). Thus, stellarators with QI fields are now tenable candidates for fusion reactors ([Lion et al. 2025; Hegna et al. 2025](#)). In designing a reactor, it is useful to understand the landscape of viable magnetic fields. However, understanding QI fields is a difficult task, as QI is fundamentally a global, topological property. QP, albeit more restrictive, is more amenable to theoretical understanding, since quasisymmetry is a local constraint.

Despite their attractive properties, quasi-poloidal magnetic fields are overlooked, often on the basis of two theoretical arguments. Firstly, there is a prevailing misconception (see, e.g., [Garren & Boozer 1991](#)) that if the radial drift vanishes pointwise, then the magnetic field strength must be constant on the flux surface, which is unreasonably constraining. This is not true, however: QP flux surfaces with zero net toroidal current also have vanishing radial drift. Granted, the only explicitly known class of magnetic fields that has geodesic field lines is the [Palumbo \(1968\)](#) magnetic fields, which do have constant field strength on the flux surfaces and are the only axisymmetric fields with this property ([Schief 2003](#)). Nonetheless, the lack of analytical QP solutions does not preclude the attainment of very accurate, numerically generated QP magnetic fields.

Secondly, exact QP is impossible close to the magnetic axis. The proof of this is reproduced in appendix A. However, this formal proof has limited relevance for practical stellarators: for low aspect ratio stellarators, the ‘near-axis’ region is much smaller than the volume enclosed by the last closed flux surface and for large aspect ratio stellarators, the level of QP-breaking around the axis can be made asymptotically small. Nonetheless, the proof indicates that we cannot replicate the success of directly constructing approximate fields using a near-axis expansion, as is possible for QI and other forms of quasisymmetry ([Landreman & Sengupta 2019; Goodman et al. 2023; Rodríguez et al. 2023; Jorge et al. 2022; Camacho Mata et al. 2022](#)). In this work, we provide an alternative analytical tool for constructing and understanding QP flux surfaces.

The principal result of this paper is a reduction of the problem of finding QP surfaces. Generally, to find a flux surface with desired properties, one has to find a particular 3D bundle of field lines, as properties such as field strength and currents depend on field lines adjacent to the flux surface. Remarkably, in the case of QP surfaces, it suffices to solve for the geometry of a particular 2D bundle of field lines. This 2D problem is not overdetermined, surprisingly simple, and can be independently used to find QP surfaces. To reveal the simplification, we describe the magnetic field within a moving frame formalism in §2. Readers primarily interested in results may skip the mathematical details of this section, but should note that much of the notation used in this paper is

defined there. In §3, we first define a local generalisation to QP surfaces, termed *local QP* (LQP) surfaces. Then, we justify the moving frame formalism by deriving the main result, the *surface equations*, which are a reduced, decoupled model for LQP surfaces. In §3.3, we sketch how the surface equations can be used to formulate a simplified surface optimisation problem for finding QP surfaces. In §4, we note two canonical classes of solutions: generalised helicoids, with surfaces of revolution (magnetic mirrors) as a notable subtype, and Hasimoto surfaces, which are surfaces traced out by the self-induced motion of a vortex filament. In the case of toroidal Hasimoto surfaces, we develop a theory of the magnetic field strength (§4.1): we show that such surfaces in vacuum are *flat mirrors* (Velasco *et al.* 2023) and derive governing equations for the field strength. In §5, the surface equations are compared with numerical magnetic field configurations optimised for QP symmetry. Using the surface equations, we explain the optimiser’s preference for cusps, narrow pinch points, and high mirror ratios.

## 2. A moving frame representation of a magnetic field

In this section, we consider an alternative description of a solenoidal field  $\mathbf{B}$ . We work in a field-line-following coordinate system  $(l, \alpha, \psi)$ , where

$$\frac{\partial \mathbf{r}}{\partial l} = \hat{\mathbf{t}} := \frac{\mathbf{B}}{B}, \quad (2.1a)$$

$$\mathbf{B} = \nabla\psi \times \nabla\alpha, \quad (2.1b)$$

where we define the tangential unit vector  $\hat{\mathbf{t}}$ . Such a field-line-following coordinate system always exists locally due to the Clebsch (1859) representation. In §3, we adopt a specific choice of field-line-following coordinates when we consider LQP surfaces.

We expand vectors in the orthonormal frame  $(\hat{\mathbf{t}}, \hat{\mathbf{n}}, \hat{\mathbf{b}})$ , where  $\hat{\mathbf{n}} = \nabla\psi/|\nabla\psi|$  is the surface normal and the binormal is  $\hat{\mathbf{b}} = \hat{\mathbf{t}} \times \hat{\mathbf{n}}$ . This is the Darboux frame (Darboux 2000) of the surfaces given by the level sets of  $\psi$ , i.e., the flux surfaces. This is shown in figure 1. Though we use the usual nomenclature, such flux surfaces are considered only locally at this stage.

We expand the covariant basis vectors in this frame:

$$\frac{\partial \mathbf{r}}{\partial \alpha} = \eta \hat{\mathbf{t}} + \rho \hat{\mathbf{b}}, \quad (2.2a)$$

$$\frac{\partial \mathbf{r}}{\partial \psi} = \lambda \hat{\mathbf{t}} + \mu \hat{\mathbf{n}} + \nu \hat{\mathbf{b}}, \quad (2.2b)$$

for some  $\eta, \rho, \lambda, \mu$ , and  $\nu$ . We have used the fact that  $\partial_\alpha \mathbf{r} \cdot \nabla\psi = 0$ . In terms of these variables,  $B = 1/\mu\rho$  and  $\nabla\psi = \hat{\mathbf{n}}/\mu$ .

The variables  $\eta, \rho, \lambda, \mu$ , and  $\nu$  constitute the metric in this coordinate system, so they are constrained by the fact that 3D Euclidean space is flat. Namely, the Riemann curvature tensor, which is a function of the metric, should vanish. Calculating such flatness conditions directly is algebraically cumbersome. Instead, we use the *method of moving frames* (Darboux 2000; Cartan 2001). Although seemingly circuitous, this method naturally provides the requisite variables for understanding the geometry of the flux surface as a surface embedded in 3D Euclidean space. In appendix B, we show the equivalence between this method and the Riemann flatness conditions.

Using the orthonormality, completeness, and smoothness of the Darboux frame  $(\hat{\mathbf{t}}, \hat{\mathbf{n}}, \hat{\mathbf{b}})$ , we can define  $\mathbf{K} = (K_1, K_2, K_3)$ ,  $\boldsymbol{\chi} = (\chi_1, \chi_2, \chi_3)$ , and  $\boldsymbol{\sigma} = (\sigma_1, \sigma_2, \sigma_3)$  such

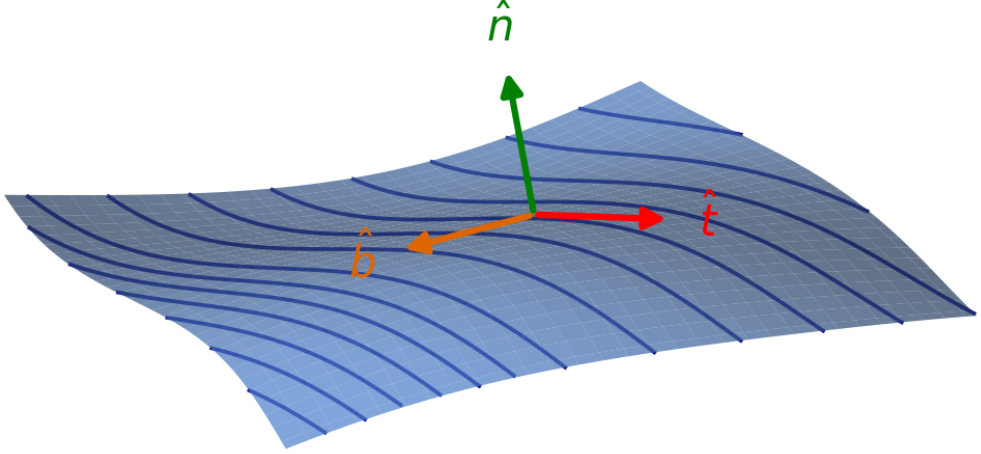


FIGURE 1. Illustration of the Darboux frame on a flux surface (constant  $\psi$ ).  $\hat{t}$  is parallel to field lines (shown in dark blue) and lies in the tangent plane to the surface,  $\hat{n}$  is normal to the surface, and  $\hat{b} = \hat{t} \times \hat{n}$  also lies in the tangent plane to the surface.

that

$$\frac{\partial}{\partial l} \begin{pmatrix} \hat{t} \\ \hat{n} \\ \hat{b} \end{pmatrix} = \begin{pmatrix} 0 & -K_3 & K_2 \\ K_3 & 0 & -K_1 \\ -K_2 & K_1 & 0 \end{pmatrix} \begin{pmatrix} \hat{t} \\ \hat{n} \\ \hat{b} \end{pmatrix}, \quad (2.3a)$$

$$\frac{\partial}{\partial \alpha} \begin{pmatrix} \hat{t} \\ \hat{n} \\ \hat{b} \end{pmatrix} = \begin{pmatrix} 0 & -\chi_3 & \chi_2 \\ \chi_3 & 0 & -\chi_1 \\ -\chi_2 & \chi_1 & 0 \end{pmatrix} \begin{pmatrix} \hat{t} \\ \hat{n} \\ \hat{b} \end{pmatrix}, \quad (2.3b)$$

$$\frac{\partial}{\partial \psi} \begin{pmatrix} \hat{t} \\ \hat{n} \\ \hat{b} \end{pmatrix} = \begin{pmatrix} 0 & -\sigma_3 & \sigma_2 \\ \sigma_3 & 0 & -\sigma_1 \\ -\sigma_2 & \sigma_1 & 0 \end{pmatrix} \begin{pmatrix} \hat{t} \\ \hat{n} \\ \hat{b} \end{pmatrix}. \quad (2.3c)$$

Relative to the field lines on the flux surface,  $-K_3$  is the normal curvature,  $K_2$  is the geodesic curvature, and  $K_1$  is the geodesic torsion (Eisenhart 2013). The anti-symmetry of the matrices follows from the orthonormality of the frame.

Compatibility of these equations in flat space requires that the partial derivatives applied to the Darboux frame commute. For example,  $\partial_l \partial_\alpha(\hat{t}, \hat{n}, \hat{b}) = \partial_\alpha \partial_l(\hat{t}, \hat{n}, \hat{b})$ . This leads to

$$\chi_l - \mathbf{K}_\alpha = \mathbf{K} \times \boldsymbol{\chi}, \quad (2.4a)$$

$$\mathbf{K}_\psi - \boldsymbol{\sigma}_l = \boldsymbol{\sigma} \times \mathbf{K}, \quad (2.4b)$$

$$\boldsymbol{\sigma}_\alpha - \boldsymbol{\chi}_\psi = \boldsymbol{\chi} \times \boldsymbol{\sigma}, \quad (2.4c)$$

where the subscripts denote partial derivatives. This is consistent with intuition in flat space: vectors parallel transported in closed loops should return to the same vector, so partial derivatives applied to vectors should commute.

Furthermore,  $\mathbf{r}_{l\alpha} = \mathbf{r}_{\alpha l}$  gives

$$\eta_l = K_2\rho, \quad (2.5a)$$

$$\chi_3 = K_3\eta - K_1\rho, \quad (2.5b)$$

$$\chi_2 = K_2\rho + \rho_l. \quad (2.5c)$$

Similarly,  $\mathbf{r}_{l\psi} = \mathbf{r}_{\psi l}$  gives

$$\lambda_l = K_2\nu - K_3\mu, \quad (2.6a)$$

$$\mu_l = K_3\lambda - K_1\nu - \sigma_3, \quad (2.6b)$$

$$\nu_l = K_1\mu - K_2\lambda + \sigma_2. \quad (2.6c)$$

Finally,  $\mathbf{r}_{\alpha\psi} = \mathbf{r}_{\psi\alpha}$  gives

$$\eta_\psi - \lambda_\alpha = \sigma_2\rho + \chi_3\mu - \chi_2\nu, \quad (2.7a)$$

$$\mu_\alpha = \sigma_1\rho - \sigma_3\eta + \chi_3\lambda - \chi_1\nu, \quad (2.7b)$$

$$\rho_\psi - \nu_\alpha = \chi_2\lambda - \chi_1\mu - \sigma_2\eta. \quad (2.7c)$$

Finding  $\eta, \rho, \lambda, \mu, \nu, \mathbf{K}, \boldsymbol{\chi}$ , and  $\boldsymbol{\sigma}$  that satisfy equations (2.4), (2.5), (2.6), and (2.7) is equivalent to specifying a solenoidal field  $\mathbf{B}$ . In the subsequent sections, we consider further properties of the magnetic field in terms of these variables.

For future reference, we also write the current  $\mathbf{J} = \nabla \times \mathbf{B}$  as

$$\begin{aligned} \mathbf{J} = \frac{1}{\mu\rho} \left[ \left( \left( \frac{1}{\mu\rho} \right)_\alpha - \left( \frac{\eta}{\mu\rho} \right)_l \right) \frac{\partial \mathbf{r}}{\partial \psi} \right. \\ \left. + \left( \left( \frac{\eta}{\mu\rho} \right)_\psi - \left( \frac{\lambda}{\mu\rho} \right)_\alpha \right) \frac{\partial \mathbf{r}}{\partial l} + \left( \left( \frac{\lambda}{\mu\rho} \right)_l - \left( \frac{1}{\mu\rho} \right)_\psi \right) \frac{\partial \mathbf{r}}{\partial \alpha} \right], \end{aligned} \quad (2.8)$$

which can be derived using the expression for the curl in general coordinates (see, e.g., [Imbert-Gerard \*et al.\* 2024](#)).

### 3. A reduced model for local QP surfaces

We define a *local QP* (LQP) surface as a flux surface where

- (i) the field lines are geodesics,
- (ii) the current normal to the surface is zero, and
- (iii) the current parallel to the field lines is zero.

These properties depend only on the local (albeit 3D) details of the magnetic field, whereas QP is a global property of a toroidal magnetic field. Nonetheless, LQP surfaces are the appropriate local generalisation of QP surfaces: force-balanced QP magnetic fields with zero enclosed toroidal current have LQP flux surfaces, as discussed in §3.1. We note that flux surfaces in magnetic mirror geometry can also be LQP surfaces.

Independently of the relationship with QP surfaces, LQP surfaces are worthy of consideration on physical grounds. That the current normal to the surface vanishes is a trivial consequence of magnetohydrostatic (MHS) force balance,

$$\mathbf{J} \times \mathbf{B} = \nabla p(\psi), \quad (3.1)$$

where we assume a scalar pressure. If the field lines are geodesics of the flux surface, the radial drift in the guiding centre approximation vanishes pointwise, resulting in no radial neoclassical transport and no bootstrap current to first order in guiding-centre

motion. The Pfirsch-Schlüter current also vanishes for geodesic field lines, so the plasma does not generate its own parallel currents; hence, it is reasonable to further assume that the parallel current is zero. Indeed, this has its own merits: negligible parallel current improves MHD stability and is one of the intrinsic advantages of a stellarator over a tokamak (Helander *et al.* 2012).

The main result of this section—and indeed of the paper—is introduced in §3.2, where we present a surprisingly simple model for producing LQP surfaces. We also sketch how this model can be used to independently generate QP surfaces (§3.3) and discuss the physics that makes LQP surfaces amenable to such simplification (§3.4).

### 3.1. Relation to quasi-poloidal symmetry

We start by examining LQP surfaces. By definition, field lines are geodesics of the surface if the geodesic curvature  $K_2$  vanishes. Physically, this is because the ‘acceleration’ term  $\partial\hat{\mathbf{t}}/\partial l$  has no component in the tangent plane of the surface, spanned by  $(\hat{\mathbf{t}}, \hat{\mathbf{b}})$ , as can be seen from equation (2.3a). By equation (2.5a), this implies  $\eta_l = 0$ , and we can therefore change coordinates from  $(l, \alpha)$  to  $(l', \alpha)$  by shifting the origin of the field lines,

$$l' := l - \int^{\alpha} d\alpha' \eta(\alpha', \psi). \quad (3.2)$$

This then implies  $\eta' = 0$ , where  $\eta'$  is defined as in equation (2.2) but now with respect to  $(l', \alpha, \psi)$  coordinates. This choice of coordinates is a particular example of *geodesic coordinates* (see, e.g., Eisenhart 2013). The coordinates  $l'$  and  $\alpha$  are orthogonal on the surface, since  $(\partial_\alpha \mathbf{r})_{l'} = \rho' \hat{\mathbf{b}}$  is perpendicular to  $(\partial_{l'} \mathbf{r})_\alpha = \hat{\mathbf{t}}$ . Henceforth, we work in such coordinates, so we drop the prime on  $l', \eta', \eta$ , etc. Thus, the geodesic condition on LQP surfaces simply becomes  $\eta = 0$ .

Additionally, by definition, the current normal to the LQP surfaces vanishes. Thus, by equation (2.8), we conclude that

$$(\mu\rho)_\alpha = 0, \quad (3.3)$$

or equivalently that  $\partial B/\partial\alpha = 0$ . This symmetry of the field strength is simply quasisymmetry. Indeed, we define the quasisymmetry vector as the covariant basis vector  $\mathbf{u} = \partial_\alpha \mathbf{r} = \rho \hat{\mathbf{b}}$ . Then, using the quasisymmetry definition of Rodríguez *et al.* (2020), it follows that locally

$$\mathbf{u} \cdot \nabla B = 0, \quad (3.4a)$$

$$\mathbf{u} \times \mathbf{B} = \nabla\psi, \quad (3.4b)$$

$$\nabla \cdot \mathbf{u} = 0. \quad (3.4c)$$

Note that equation (3.4b) usually has an additional minus sign, but we define  $\mathbf{u}$  such that  $\rho > 0$  and  $(\hat{\mathbf{t}}, \hat{\mathbf{n}}, \hat{\mathbf{b}})$  forms a right-handed coordinate system. It is notable that we did not have to assume quasisymmetry; it emerged naturally from assuming geodesic field lines and zero current normal to the surfaces and revealed itself in geodesic coordinates.

We now demonstrate why QP surfaces are natural choices for LQP surfaces. We prove that, given a toroidal surface with zero enclosed toroidal current and pointwise zero normal current, the field lines are geodesics on that surface if and only if the magnetic field strength on the surface has QP symmetry.

Firstly, we prove the forward direction: geodesic field lines imply QP. We have already shown that LQP surfaces are quasisymmetric, so they possess a symmetry vector  $\mathbf{u}$  and a corresponding symmetry coordinate  $\alpha$ . On a toroidal surface where  $B$  is not constant on a flux surface, the integral curves of  $\mathbf{u}$  must close, according to equation (3.4a). The

integral of  $\mathbf{B}$  around a closed  $\mathbf{u}$  integral curve (denoted  $\partial S$ ) must vanish because  $\mathbf{u} \cdot \mathbf{B} = 0$  by the choice of geodesic coordinates, so

$$0 = \oint_{\partial S} d\alpha \frac{\partial \mathbf{r}}{\partial \alpha} \cdot \mathbf{B} \quad (3.5a)$$

$$= \iint_S dS \cdot \mathbf{J} \quad (3.5b)$$

where the second line follows from Stokes' theorem. Because the poloidal current exterior to the flux surface does not vanish, whereas the toroidal current enclosed by the flux surface does vanish,  $\partial S$  must close poloidally. This yields QP.

We now show the backward direction: QP implies geodesic field lines, given zero enclosed toroidal current and  $\mathbf{J} \cdot \hat{\mathbf{n}} = 0$ . By quasisymmetry and the vanishing of the normal current, we have  $(\eta/\mu\rho)_l = 0$ . For an irrational surface, this means that  $\eta/\mu\rho$  is constant on the surface, since field lines get arbitrarily close to every point on the surface. For rational surfaces, assuming that the rotational transform is not constant and we have QP in an infinitesimal volume around the surface, we also have that  $\eta/\mu\rho$  is constant by continuity. Then, we integrate the magnetic field along the poloidal symmetry curve  $\partial S$ . Using that the enclosed toroidal current vanishes and Stokes' theorem, this integral vanishes:

$$0 = \oint_{\partial S} d\alpha \frac{\partial \mathbf{r}}{\partial \alpha} \cdot \mathbf{B} \quad (3.6a)$$

$$= \oint_{\partial S} d\alpha \frac{\eta}{\mu\rho}. \quad (3.6b)$$

As  $\eta/\mu\rho$  is constant, this implies that  $\eta = 0$ , and consequently that we have geodesic field lines.

In appendix C, we make the connection with Boozer (1981) coordinates, which can be defined since  $\mathbf{J} \cdot \hat{\mathbf{n}} = 0$  (Rodríguez *et al.* 2021). We also show that, under the further assumption of MHS force balance, the parallel current on a QP surface vanishes whenever the enclosed toroidal current vanishes. Thus, we conclude from this subsection that QP is the natural global analogue for LQP surfaces. However, LQP surfaces, defined locally, constitute a larger class of possible surfaces, toroidal or not (e.g., magnetic mirrors).

### 3.2. The surface equations

In this subsection, we present a reduced, decoupled model for single LQP flux surfaces. We first discuss what it means to have defined a single LQP surface in the language of the moving frame.

A magnetic field is exactly described by  $\eta, \rho, \lambda, \mu, \nu, \mathbf{K}, \chi$ , and  $\sigma$  as functions of  $(l, \alpha, \psi)$ , provided that the geometric constraints of §2 are obeyed. In contrast, a single flux surface, taken as an embedded surface in real space, is precisely described by  $\eta, \rho, \mathbf{K}$ , and  $\chi$  as functions of  $(l, \alpha)$ , provided that equations (2.4a) and (2.5) are satisfied. This result of classical differential geometry is referred to as Bonnet's theorem. A magnetic field requires additional information because it is a 3D bundle of field lines, whereas a single flux surface is a 2D manifold.

Even if we consider only a single LQP flux surface, finding an LQP surface is in principle a 3D problem. This is because defining the field strength and current on a flux surface requires information about field lines away from that surface. For the field strength, given  $B = 1/(\mu\rho) = 1/(\mathbf{r}_l \cdot \mathbf{r}_\alpha \times \mathbf{r}_\psi)$ , we need to know field lines in the infinitesimal neighbourhood of the surface, i.e., we need to know  $\mathbf{r}(l, \alpha, \psi_0 + \delta\psi)$  to first order in  $\delta\psi$ , where  $\psi_0$  labels the relevant flux surface.

In general, describing currents on a flux surface requires information about field lines further from the surface, i.e.  $\mathbf{r}(l, \alpha, \psi_0 + \delta\psi)$  to two orders in  $\delta\psi$ . This is manifest in the expression (2.8) for the current as terms like  $\mu_\psi$  depend on  $\mathbf{r}_{\psi\psi}$  (see equation (2.2b)). However, when the field lines are geodesics on the surface, one requires information only about field lines in the immediate infinitesimal neighbourhood, i.e. to first order in  $\delta\psi$ , to define the currents normal to the surface and parallel to the field lines. This is because when  $\eta = 0$  on the flux surface, which is the geodesic condition in geodesic coordinates as described in §3.1, there are no terms involving  $\mathbf{r}_{\psi\psi}$  contributing to the normal and parallel current, as can be seen from equation (2.8).

Therefore, to define a single LQP surface, we need to define a particular  $\mathbf{r}(l, \alpha, \psi_0 + \delta\psi)$  to first order in  $\delta\psi$ . In other words, a single LQP surface is defined by field lines on and directly adjacent to that surface. Geometrically, defining such field lines is equivalent to providing  $\lambda, \mu, \nu$ , and  $\sigma$  on the surface as functions of  $(l, \alpha)$  at fixed  $\psi = \psi_0$  and  $\mathbf{K}, \mathbf{x}, \rho$ , and  $\eta$  as functions of  $(l, \alpha, \psi_0 + \delta\psi)$ , provided that equations (2.4), (2.6), and (2.7) hold at  $\psi = \psi_0$  and equations (2.5) hold for  $\psi = \psi_0 + \delta\psi$ . Solving these equations for those variables merely provides the requisite structure; an LQP surface must also satisfy the physical constraints of having (i) geodesic field lines, (ii) zero normal current, and (iii) zero parallel current:

$$\eta = 0 \quad \text{for } \psi = \psi_0 + \delta\psi, \quad (3.7a)$$

$$(\mu\rho)_\alpha = 0 \quad \text{for } \psi = \psi_0, \quad (3.7b)$$

$$\lambda_\alpha = 0 \quad \text{for } \psi = \psi_0. \quad (3.7c)$$

The first equation corresponds to having geodesic field lines and choosing  $(l, \alpha)$  to be geodesic coordinates (as discussed in §3.1). We do not just impose  $\eta = 0$  on the relevant flux surface, but also in the neighbourhood of the flux surface. This reflects the requirement that a finite volume of surfaces possess the physical benefits of geodesic field lines. The second equation corresponds to zero normal current and is equivalent to quasisymmetry (also discussed in §3.1). Given the previous two equations, the third equation corresponds to zero parallel current on the relevant flux surface.

We note one crucial simplification arising from field lines being geodesics. By equation (2.5a), we deduce that  $K_2 = 0$ . Thus, the Darboux frame on the surface reduces to the Frenet-Serret frame for the field lines, since equation (2.3a) becomes the Frenet-Serret formulae (Serret 1851; Frenet 1852). To comply with the usual notation, we replace ‘ $\mathbf{K}$ ’ with the curvature  $\kappa := -K_3$  (equal to the normal curvature) and torsion  $\tau := -K_1$ . We note that the curvature defined in this way can be negative, precisely when the principal normal of the field lines is anti-aligned with the surface normal.

We have determined the relevant variables and equations for finding a single LQP surface using the moving frame formalism. In appendix D, we manipulate and reduce these equations to obtain the main result of this paper: the geometry of a single LQP flux surface is determined by the solution to the *surface equations*

$$\kappa_\alpha = -2\rho_l\tau - \rho\tau_l, \quad (3.8a)$$

$$\tau_\alpha = \rho_l\kappa + \left( \frac{\rho_{ll} - \rho\tau^2}{\kappa} \right)_l, \quad (3.8b)$$

$$\left( \frac{\kappa}{\rho} \right)_\alpha = 0. \quad (3.8c)$$

For the reader who skipped to these equations, we reiterate that  $\kappa$  is the signed curvature of the field lines,  $\tau$  is the torsion of the field lines,  $(l, \alpha)$  are a particular choice of field-

line-following coordinates where  $\partial_\alpha \mathbf{r} = \mathbf{u}$  is the quasisymmetry vector, and  $\rho = |\mathbf{u}|$  is the ‘orthogonal distance’ between the field lines.

The surface equations have three remarkable properties. Firstly, the surface equations depend only on the geometry of the flux surface and the field lines on that flux surface (through the variables  $(\rho, \kappa, \tau)$ ); they do not depend on field lines away from the flux surface. How can this be if the field strength and currents on the flux surface depend on field lines away from the flux surface? This is because of a second remarkable property: given a solution to the surface equations (representative of an embedded surface foliated by field lines), there exist (at least locally) some neighbouring field lines that would confer upon the surface the relevant LQP properties of zero normal and parallel currents. We show this mathematically by providing a set of equations that (along with the surface equations) are equivalent to the original problem for finding an LQP surface, and then showing that these equations admit solution. These equations are derived alongside the surface equations in appendix D and are presented here:

$$\eta = 0, \tag{3.9a}$$

$$K_2 = 0, \tag{3.9b}$$

$$\chi_1 = -\frac{\rho_{ll} - \rho\tau^2}{\kappa}, \tag{3.9c}$$

$$\chi_2 = \rho_l, \tag{3.9d}$$

$$\chi_3 = \rho\tau, \tag{3.9e}$$

$$\lambda_\alpha = 0, \tag{3.9f}$$

$$\lambda_l = \kappa\mu, \tag{3.9g}$$

$$\nu_l = \frac{\rho_l}{\rho}\nu - 2\tau\mu, \tag{3.9h}$$

$$\mu_\alpha = -\frac{\rho_\alpha}{\rho}\mu, \tag{3.9i}$$

$$\sigma_1 = -\frac{\rho_\alpha}{\rho^2}\mu - \tau\lambda - \frac{\nu}{\rho}\frac{\rho_{ll} - \rho\tau^2}{\kappa}, \tag{3.9j}$$

$$\sigma_2 = \frac{\rho_l}{\rho}\nu - \tau\mu, \tag{3.9k}$$

$$\sigma_3 = -\mu_l - \kappa\lambda + \tau\nu, \tag{3.9l}$$

$$\rho_\psi = \nu_\alpha + \rho_l\lambda + \frac{\rho_{ll} - \rho\tau^2}{\kappa}\mu, \tag{3.9m}$$

$$\eta_\psi = 0, \tag{3.9n}$$

$$\kappa_\psi = \mu_{ll} + (\kappa^2 + 3\tau^2)\mu + \kappa_l\lambda + \frac{\kappa_\alpha}{\rho}\nu, \tag{3.9o}$$

$$\tau_\psi = \frac{\tau_\alpha}{\rho}\nu + \tau_l\lambda + \frac{\rho_\alpha}{\rho^2}\mu_l + \left( \left( \frac{\rho_\alpha}{\rho^2} \right)_l - 2\frac{\tau}{\rho}\frac{\rho_{ll} - \rho\tau^2}{\kappa} \right)\mu, \tag{3.9p}$$

$$K_{2\psi} = 0, \tag{3.9q}$$

$$\chi_{1\psi} = -\left( \frac{\rho_{ll} - \rho\tau^2}{\kappa} \right)_\psi, \tag{3.9r}$$

$$\chi_{2\psi} = \rho_{l\psi}, \tag{3.9s}$$

$$\chi_{3\psi} = (\rho\tau)_\psi. \tag{3.9t}$$

These equations apply at fixed  $\psi = \psi_0$ . We now justify why these equations are

solvable, given a solution  $(\rho, \kappa, \tau)$  to the surface equations. First, we consider the variables  $(\lambda, \mu, \nu)$ . They are determined by the homogeneous, linear differential equations (3.9f)–(3.9i). By the [Frobenius \(1877\)](#) theorem, there exists a solution  $(\lambda, \mu, \nu)$  to these differential equations. This is because equations (3.9f) and (3.9g) are compatible: both equations agree that  $\lambda_{\alpha l} = 0$ , since  $(\kappa\mu)_\alpha = 0$  by the surface equation (3.8c) and the quasisymmetry condition, presented here as equation (3.9i). The remaining functions  $(\eta, K_2, \chi, \sigma, \rho_\psi, \eta_\psi, \tau_\psi, \mathbf{K}_\psi, \chi_\psi)$  are algebraically and compatibly determined in terms of  $\rho, \kappa, \tau, \lambda, \mu$ , and  $\nu$  by equations (3.9a)–(3.9e) and (3.9j)–(3.9t).

A solution to these equations, alongside a solution to the surface equations, represents a single LQP flux surface. This is because, as discussed, a single LQP surface is defined by field lines in an infinitesimal volume around that surface, or equivalently, by the functions  $\lambda, \mu, \nu, \sigma, \mathbf{K}, \chi, \rho, \eta, \mathbf{K}_\psi, \chi_\psi, \rho_\psi$ , and  $\eta_\psi$  at fixed  $\psi = \psi_0$  as functions of  $(l, \alpha)$ . Thus, the problem of finding an LQP flux surface has been reduced to solving the surface equations, since the remaining part of the problem is solvable given a solution to the surface equations. It is surprising that we do not have an overdetermined system, despite the numerous equations involved. We discuss the physical reasons for this in §3.4.

A third and final remarkable property of the reduction to the surface equations is that  $(\rho, \kappa, \tau)$  *completely determine* the surface and the field lines on it. Intuitively, this is clear:  $(\kappa, \tau)$  determine the field lines individually, and  $\rho$  tells us the spacing between the field lines. Formally, we can recall Bonnet's theorem (stated at the start of this subsection) and note that  $\chi$  is algebraically determined by  $(\rho, \kappa, \tau)$  through equations (3.9c)–(3.9e). The relevant compatibility conditions (2.4a) and (2.5) are satisfied identically when  $\chi$  is expressed in this way, with the exception of two components of (2.4a), which are equivalent to the first two surface equations. Thus, the first two surface equations are purely geometric conditions, as viewed by geodesics. Curiously, the physics of vanishing normal and parallel current reduces to the simple equation (3.8c).

To summarise this subsection, the problem of finding an LQP surface has been reduced from a 3D problem to a 2D problem, since we need only solve the surface equations for the geometry of an embedded surface. An LQP surface is defined by its properties of field strength and currents, which depend on field lines away from the surface. However, once we have a solution to the surface equations, we can locally guarantee that there exist neighbouring field lines that would give that surface the relevant properties of an LQP flux surface, viz. zero parallel and normal currents. We can make this guarantee because the variables that define the neighbouring field lines can be found by solving a well-posed set of equations. In this sense, the surface equations are decoupled and complete. Appendix E makes a connection with the language of classical differential geometry, for the reader who is fluent in such a language.

Finally, we comment on magnetohydrostatic (MHS) force balance (3.1), which depends on the current in the binormal direction (perpendicular to the field lines and tangential to the flux surface). This component of current has not yet been considered and need not vanish, unlike the parallel and normal components of current. By substituting the expression (2.8) for the current into MHS force balance (3.1), we find

$$\mu_\psi = -\frac{\rho_\psi}{\rho} \mu + p'(\psi) \rho^2 \mu^3 - \rho \mu^2 \left( \frac{\lambda}{\mu \rho} \right)_l. \quad (3.10)$$

Because we look for a solution on a single surface, (3.10) does not lead to overdetermination, since  $\mu_\psi$  was unconstrained by the system of equations in (3.9). Physically, this is because the current in the binormal direction is affected by field lines even further from the surface. Formally, the presence of  $\mu_\psi$  in the expression for this component of the

current implies that one requires  $\mathbf{r}(l, \alpha, \psi_0 + \delta\psi)$  to two orders in  $\delta\psi$  to define  $\mathbf{J} \cdot \hat{\mathbf{b}}$  on the flux surface  $\psi = \psi_0$ . For a single LQP flux surface, these ‘far away’ field lines do not affect the parallel or normal currents, so we can choose them to satisfy MHS force balance on the relevant surface: hence, there is no overdetermination by imposing force balance when considering a single LQP flux surface. This is a fortunate and unique scenario: typically in studies of MHS equilibria, imposing MHS force balance on a quasisymmetric equilibrium creates overdetermination (Garren & Boozer 1991; Sengupta *et al.* 2024). Moreover, equation (3.10) implies that  $(\mu\rho)_{\psi\alpha} = 0$ , which is just a statement of quasisymmetry in the neighbourhood of the surface. Therefore, all considerations thus far, including the surface equations, are consistent with a finite-beta equilibrium.

### 3.3. Solving the surface equations through optimisation

In this subsection, we sketch how the surface equations could be solved as an optimisation problem for generating LQP flux surfaces. This could be used as part of a larger optimisation for generating a practical QP stellarator field or for quickly and efficiently generating flux surfaces to study trends in QP equilibria. This approach would be intrinsically faster than usual MHD equilibrium solvers (e.g., VMEC, Hirshman & Whitson 1983, or DESC, Dutt & Kolemen 2020) because the free parameters are 2D instead of 3D. For concreteness, we take the example of a toroidal QP flux surface, but this process applies equally to, say, the generation of asymmetric magnetic mirror flux surfaces with the desirable properties of an LQP surface.

Computationally, we work in the coordinate system  $(\vartheta, \varphi)$ , where  $\varphi$  is some particular toroidal angle coordinate and  $\vartheta$  is some particular poloidal angle coordinate. The flux surface is parameterised by the single-valued functions  $R(\vartheta, \varphi)$  and  $Z(\vartheta, \varphi)$ , where  $R$  and  $Z$  correspond to the usual cylindrical coordinates with respect to an axis passing through the centre of the torus. In practice, one could work in discrete Fourier modes of  $(\vartheta, \varphi)$ , e.g.,  $R_{mn}$ , up to some chosen level of precision.

On the toroidal surface, we also parameterise a foliation of closed poloidal loops. In the particular  $(l, \alpha)$  coordinate system used throughout this paper, these correspond to lines of constant  $l$ . Equivalently, they are the field lines for the field  $\mathbf{u} = \partial_\alpha \mathbf{r}$ , or the loops along which the magnetic field strength would be constant (though we do not solve for the magnetic field strength in this 2D problem). The field lines are taken as perpendicular to these poloidal loops. We take the poloidal loops to be level sets of some function  $\Lambda(\vartheta, \varphi)$ , which is necessarily periodic in  $\vartheta$ . For specificity, we could take  $\Lambda$  to be the distance along a chosen field line from some reference poloidal loop. In the solved problem where the field lines are geodesics, this  $\Lambda$  becomes independent of the chosen field line and is equivalent to our choice of arc length coordinate  $l$ .

We generate LQP flux surfaces by solving the surface equations as an optimisation problem. The free parameters are the surface, through  $R(\vartheta, \varphi)$  and  $Z(\vartheta, \varphi)$ , and the poloidal loops, through the function  $\Lambda(\vartheta, \varphi)$ . The function  $\Lambda(\vartheta, \varphi)$  is constrained to have level sets that close poloidally. The cost function,  $f[\Lambda, R, Z]$ , has two parts,  $f_1[\Lambda, R, Z]$  and  $f_2[\Lambda, R, Z]$ , where  $f_1[\Lambda, R, Z] = 0$  ensures that the field lines are geodesics and if  $f_2[\Lambda, R, Z] = 0$  also, the third surface equation, (3.8c), is solved. We now consider these two parts in more detail.

Firstly, we enforce that the field lines are geodesics. The tangent vector to the field lines  $\hat{\mathbf{t}}$  is obtained by calculating the orthogonal to the poloidally closed level sets of  $\Lambda$ . The orthogonal direction in  $(\vartheta, \varphi)$  space depends on  $R$  and  $Z$  and can be calculated via well-established methods. Then, using the tangent vector field  $\hat{\mathbf{t}}$ , the geodesic curvature can be calculated, in a way that likewise depends on  $R$  and  $Z$  and is also calculable via well-established methods. The field lines are geodesics if and only if the geodesic

curvature is zero everywhere, so we take this part of the cost function to be

$$f_1[\Lambda, R, Z] = \int_0^{2\pi} d\vartheta \int_0^{2\pi} d\varphi \sqrt{g}_{\text{surf}} |\kappa_g|, \quad (3.11)$$

where  $\kappa_g \equiv K_2$  is the geodesic curvature and the surface Jacobian  $\sqrt{g}_{\text{surf}}$  ensures the integral is a surface average.

The second part of the cost function is connected with the third surface equation (3.8c) and is somewhat more subtle. We define the field line label  $\tilde{\alpha}$  to be constant along the magnetic field lines and go from 0 to  $2\pi$  (for specificity) along the closed poloidal loops. We then take  $s$  to be the arc length along the closed poloidal loop and define  $\tilde{\rho} := \partial s / \partial \tilde{\alpha}$ . For the third surface equation, we must also calculate the normal curvature  $\kappa_n \equiv -K_3$  from  $\hat{\mathbf{t}}$ . When the geodesic curvature is zero, the normal curvature is the same as the curvature  $\kappa$ .

We take the second part of the cost function to be

$$f_2[\Lambda, R, Z] = \int_0^{2\pi} d\vartheta \int_0^{2\pi} d\varphi \sqrt{g}_{\text{surf}} \left| \left( \ln \frac{\kappa_n}{\tilde{\rho}} \right)_{l\tilde{\alpha}} \right|. \quad (3.12)$$

To justify this expression, we show that precisely when

$$\left( \ln \frac{\kappa}{\tilde{\rho}} \right)_{l\tilde{\alpha}} = 0, \quad (3.13)$$

there exists a transformation  $\alpha = f(\tilde{\alpha})$  such that the third surface equation (3.8c) is satisfied. To show this, we suppose equation (3.13) is true. Then,

$$\left( \ln \frac{\kappa}{\tilde{\rho}} \right)_{\tilde{\alpha}} = g(\tilde{\alpha}), \quad (3.14)$$

for some particular  $g$ . Subsequently, defining  $\alpha = f(\tilde{\alpha})$ , we take  $f$  as a solution to

$$\frac{d^2 f}{d\tilde{\alpha}^2} = \frac{df}{d\tilde{\alpha}} g(\tilde{\alpha}). \quad (3.15)$$

Thus, using  $\rho = \tilde{\rho} \frac{df}{d\tilde{\alpha}}$ , the third surface equation (3.8c) is satisfied. In the 2D picture, there is a ‘gauge’ freedom  $\alpha \rightarrow f(\alpha)$  (corresponding to  $\rho \rightarrow \rho/f'(\alpha)$ ) in the orthogonal coordinate  $\alpha$ , but the third surface equation (3.8c) still imposes a non-trivial constraint, through equation (3.13).

We do not need to verify the first two surface equations, (3.8a) and (3.8b). These are identically satisfied when the field lines are geodesics, with  $\kappa = \kappa_n$  and  $\rho \rightarrow \tilde{\rho}$ . Indeed, these two surface equations are purely geometric constraints and are satisfied by any geodesic foliation of an embedded surface. In this setup, the geometry is encoded through  $R(\vartheta, \varphi)$  and  $Z(\vartheta, \varphi)$ .

We also note that in practice, solving for  $f_2[\Lambda, R, Z] = 0$  makes sense only if the field lines are sufficiently close to geodesics (i.e.,  $\kappa_n \gg \kappa_g$ ). In a computational optimisation problem, this could be achieved by including the  $f_2$  part only when  $f_1$  is sufficiently small.

In practice, once a toroidal surface has been selected by this method, it can be used as the boundary for a complete equilibrium solver. In vacuum, the boundary shape completely determines the magnetic field inside the boundary. However, because of the locality of the assumptions behind LQP surfaces, there is no guarantee that there are nested QP flux surfaces within the boundary of a surface selected by this method. In this case, a second optimisation, using the equilibrium solver, could be used to fine-tune

the boundary surface to give the desired global properties. Similar considerations would apply to finite-beta QP equilibria.

### 3.4. What is so special about LQP surfaces?

There are two unique features of LQP surfaces that lead to the drastic simplification of the surface equations. Indeed, such a reduction cannot be found generally. If we were to impose only quasisymmetry as a physical constraint (i.e., only equation (3.7b)), the moving frame formalism would lead to equations that are highly coupled and overdetermined. In such cases, describing the magnetic field through a moving frame is not particularly useful.

The first special feature is that, for LQP surfaces, the surface geometry is decoupled from the magnetic field strength. In the case of general quasisymmetry with zero normal current,  $\mathbf{u} \cdot \mathbf{B} = \eta/\mu\rho$  is constant on a flux surface (Rodríguez *et al.* 2020). This couples a quantity that influences the geometry of the flux surface,  $\eta$ , with a quantity that is determined by field lines in the neighbourhood of the surface, namely the field strength  $1/\mu\rho$ . LQP surfaces avoid this coupling by having geodesic field lines, which implies  $\eta = 0$  everywhere. Notably, given a single LQP surface, it is always possible to construct another LQP surface with the same flux surface shape but a different magnetic field strength profile (so long as  $\partial B/\partial\alpha = 0$ ). This is because we can take a complete solution to the LQP equations (3.8) and (3.9), and construct another solution through  $\mu \rightarrow g(l)\mu$  for arbitrary function  $g$ .

There is a second way in which LQP surfaces are special. Without assuming geodesic field lines, the general expression for the parallel current in the moving frame representation is

$$J_{\parallel} = \frac{1}{\mu\rho} \left( \left( \frac{\eta}{\mu\rho} \right)_{\psi} - \left( \frac{\lambda}{\mu\rho} \right)_{\alpha} \right) + \frac{\eta}{\mu\rho} \left( \left( \frac{\lambda}{\mu\rho} \right)_l - \left( \frac{1}{\mu\rho} \right)_{\psi} \right), \quad (3.16)$$

where we have continued to assume that the normal current vanishes. As an aside, the second set of terms is the Pfirsch-Schlüter current, which vanishes for geodesic field lines ( $\eta = 0$ ). For  $\eta = 0$ , the expression for the parallel current ceases to depend on  $\mu_{\psi}$ . This means that for the particular case of geodesic field lines, the parallel current is determined only by field lines in the immediate neighbourhood of the surface, not by field lines at second order from the surface. Despite being more restrictive—there are fewer field lines that can contribute to having zero parallel current—this fact leads to mathematical simplification, since the equations are decoupled from field lines that are not in the immediate neighbourhood of the surface. In other words, in the general non-geodesic case, we have to consider a ‘thicker’ volume around the surface in order to evaluate the parallel current, which means there are more variables coupled into the equations (though optimistically, this also represents increased freedom). It is also this fact that means our single LQP surface can always be force-balanced without additional overdetermination, since the binormal current  $\mathbf{J} \cdot \hat{\mathbf{b}}$  can be manipulated without affecting the parallel current, by altering field lines further from the surface through  $\mu_{\psi}$ , in accordance with equation (3.10).

## 4. On global solutions to the surface equations

We have thus far considered only local details of the magnetic field, except in §3.3, where we used the surface equations to define a reduced optimisation problem for finding toroidal QP flux surfaces. Here, we analytically apply global considerations to the surface equations. In this section, we identify two natural classes of solutions to the surface

equations: the first contains ‘magnetic mirrors’ as a solution, and the second has attractive and analytically tractable field strength properties.

We consider searching for toroidal, QP solutions. A toroidal QP surface is foliated by closed poloidal loops. Along these loops, the magnetic field strength is constant, the covariant basis vector  $\partial_\alpha \mathbf{r}$  (also the quasisymmetry vector) is tangent, and the field lines are orthogonal. In the  $(l, \alpha)$  coordinate system, these loops are given by  $l = \text{const.}$  (In §3.3, these poloidal loops were part of the free parameters for the optimisation problem.) We take  $L$  to be the distance along a field line until it returns to the same poloidal loop, this value being independent of the chosen field line. Equivalently,  $L$  is the distance along a field line between  $\phi = 0$  and  $\phi = 2\pi$  for Boozer angle  $\phi$ , as defined in appendix C.

From the first and third surface equations (3.8a) and (3.8c), we have the ‘conservation law’

$$\frac{\partial}{\partial \alpha} \left( \frac{\rho \kappa}{2} \right) + \frac{\partial}{\partial l} (\rho^2 \tau) = 0. \quad (4.1)$$

We integrate this equation around one of the closed poloidal loops, which gives

$$\oint d\alpha \rho^2 \tau = C, \quad (4.2)$$

where  $C$  is some constant, and we have used the fact that  $(\rho, \kappa, \tau)$  are single-valued. We define  $\gamma := \kappa/\rho$ , which is independent of  $\alpha$  by the third surface equation (3.8c). Then,

$$\oint d\alpha \kappa^2 \tau = C \gamma^2. \quad (4.3)$$

The left-hand side of this equation is invariant under  $l \rightarrow l + L$ , since  $\kappa$  and  $\tau$  are single-valued, so  $\gamma(l)$  is periodic with period  $L$ . This is evidently true for an irrational surface, which is one where the rotational transform  $\iota$  is irrational. This is because  $(l + L, \alpha)$  and  $(l, \alpha + 2\pi\iota)$  are the same point on the surface,  $\gamma$  is smooth and independent of  $\alpha$ , and positive integer multiples of an irrational, taken modulo  $2\pi$ , are dense in  $[0, 2\pi]$ .

The fact that  $\gamma$  is periodic and  $(\rho, \kappa, \tau)$  are generally aperiodic couples periodic and aperiodic terms in the first two surface equations (3.8a) and (3.8b). This complicates the route to a global, toroidal solution, but a separation of variables can be achieved by substituting  $\kappa = \rho\gamma$ . Then, we have

$$\gamma = -\frac{2\rho_l \tau + \rho \tau_l}{\rho_\alpha}, \quad (4.4a)$$

$$\gamma_l = \frac{K + \tau^2}{\gamma \rho_l \rho - \tau_\alpha - \frac{K + \tau^2}{\gamma}}, \quad (4.4b)$$

where  $K := -\rho_{ll}/\rho$  is the Gaussian curvature. Solving these two equations analytically in complete generality is not feasible, so we consider some natural classes of solutions. Given that  $\gamma$  is periodic in  $l$ , two natural classes emerge: a)  $(\rho, \kappa, \tau)$  are independent of  $\alpha$ , and b)  $\gamma$  is constant.

Case a) corresponds to generalised helicoids, as proved in appendix F. An example is illustrated in figure 2. In the further special case where  $\tau = 0$ , we either have surfaces of revolution with the meridians as field lines (magnetic mirrors), as illustrated in figure 3, or the surface traced out by a planar curve translated in the direction of the curve’s binormal (i.e., surfaces of the form  $z = f(x)$  with field lines given by  $y = \text{const.}$ ). These two cases are the only LQP surfaces where the torsion of the field lines is zero, even if we were to allow for  $\alpha$ -dependence. Notably, all LQP surfaces where  $\mathbf{u}$  can be extended to a Killing vector of 3D Euclidean space reduce to case a). This is also shown in appendix F.

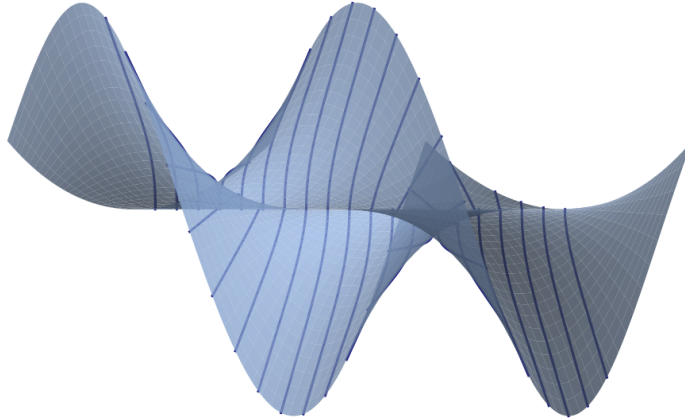


FIGURE 2. An example of a generalised helicoid, with  $\mathbf{r} = (-0.6u^2 \cos b, -0.6u^2 \sin b, u + b)$  for  $u \in [-2, 2]$  and  $b \in [0, 2\pi]$ . The magnetic field lines (shown in dark blue) are geodesics orthogonal to the helices given by  $u = \text{const}$ .

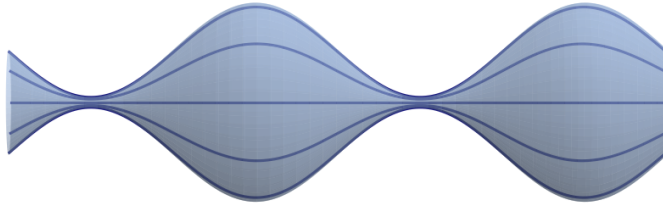


FIGURE 3. An example of a surface of revolution, with  $\mathbf{r} = ((1 + 0.9 \sin u) \cos b, (1 + 0.9 \sin u) \sin b, u)$  for  $u \in [-2\pi, 2\pi]$  and  $b \in [0, 2\pi]$ . The field lines are the meridians, highlighted in dark blue.

Thus, case a) does not include any toroidal solutions. Nonetheless, in §5, we see that numerically generated QP equilibria have sections that resemble magnetic mirrors, and in appendix I, we perturb around surfaces of revolution to qualitatively explain some properties of the toroidal equilibria.

We now consider case b). In this case,  $\rho \propto \kappa$ . We have the same physical situation under the simultaneous rescaling  $\alpha \rightarrow C\alpha$  and  $\psi \rightarrow \psi/C$  for arbitrary constant  $C$ , so we can set  $\gamma = 1$  and  $\rho = \kappa$ . With  $\rho = \kappa$ , the first two surface equations (3.8a) and (3.8b) reduce to the Da Rios-Betchov equations (Da Rios 1906; Betchov 1965), whilst the third equation (3.8c) becomes trivial. Equivalently, using the definition of  $\rho$ , we can model the field lines as obeying the vortex filament equation (also known as the localised induction approximation),

$$\frac{\partial \mathbf{r}}{\partial \alpha} = \kappa \hat{\mathbf{b}}, \quad (4.5a)$$

$$= \frac{\partial \mathbf{r}}{\partial l} \times \frac{\partial^2 \mathbf{r}}{\partial l^2}, \quad (4.5b)$$

where (4.5b) assumes that the principal normal and surface normal are in the same direction. If they are opposed, we still have the same physical equation, but under a ‘time-reversal’  $\alpha \rightarrow -\alpha$ . Surfaces traced out by a vortex filament are known as *Hasimoto surfaces*, and we appropriately adopt this term for describing LQP surfaces where  $\rho \propto \kappa$ .

Under the Hasimoto (1972) map, the Da Rios-Betchov equations are equivalent to the *nonlinear Schrödinger equation*.

The vortex filament equation, and its equivalent formulations, reappear in a variety of physical contexts. True to its name, it models the self-induced dynamics of a vortex filament in an incompressible, inviscid fluid (Da Rios 1906; Batchelor 1967). In addition, the equation appears as the continuum approximation to a discrete spin chain with interactions between neighbouring spins—the Heisenberg model (Lakshmanan 1977). The nonlinear Schrödinger equation often appears as a governing equation for dispersive, weakly nonlinear waves, such as in optical fibres (see, e.g., Biswas *et al.* 2010), deep surface gravity waves (Zakharov 1968), and Langmuir waves in hot plasmas (Oraevskii 1962). Furthermore, the nonlinear Schrödinger equation has the notable mathematical property of being an *integrable PDE* (Gardner *et al.* 1967). Rogers & Schief (2002) present diagrammatic examples of non-toroidal Hasimoto surfaces constructed out of soliton and breather solutions to the nonlinear Schrödinger equation.

The authors are aware of one known class of irrational, toroidal, Hasimoto surfaces. This solution already has prominence in an analytic MHS equilibrium, viz. the Palumbo (1968) configuration. The Palumbo configuration (or class of configurations) is an axisymmetric torus, made up of nested toroidal Hasimoto flux surfaces, with constant field strength on each surface. Remarkably, the Palumbo configuration is exact for an entire volume (not just a surface) and obeys the MHS force balance throughout for an arbitrary pressure profile  $p(\psi)$ . This series of toroidal Hasimoto surfaces is given by the periodic travelling wave solutions to the Da Rios-Betchov equations,  $\kappa = \kappa(l + c\alpha)$  and  $\tau = \tau(l + c\alpha)$ , as identified by Kida (1981). The equation for such surfaces is given in an MHS context by equation (5.26) in Schief (2003) and the surfaces are plotted in figure 1 therein. Unfortunately for our purposes, such surfaces, even when taken individually, cannot be QP, since the orthogonals to the geodesics wind helically and generally do not close. However, there may exist other toroidal Hasimoto surfaces that are consistent with QP, at least to an acceptable level of accuracy. In such a case, we can make additional statements about the magnetic field strength on such a surface, as we show in the next subsection.

#### 4.1. The magnetic field strength on toroidal Hasimoto surfaces

We have thus far ignored the magnetic field strength profile. This was because, as discussed in §3.4, the question of field strength decouples from the question of surface geometry. However, with some additional weak assumptions, we can make further statements about the magnetic field strength on Hasimoto surfaces. We first establish a connection between Hasimoto surfaces and an attractive property for practical stellarators, termed the flat mirror property. We then derive an exact governing differential equation that determines the magnetic field strength profile in terms of the surface geometry quantities,  $(\rho, \kappa, \tau)$ .

Firstly, we show that a Hasimoto surface in vacuum is a *flat mirror*, as defined and studied in Velasco *et al.* (2023). Velasco *et al.* show that such magnetic fields exhibit small radial transport of energy and good confinement of bulk and fast ions. A flat mirror is defined as a magnetic field satisfying

$$\partial_\psi (B_{\max} - B_{00}) = 0, \quad (4.6)$$

where  $B_{00} = \iint d\theta d\phi B / 4\pi^2$ , with  $(\theta, \phi)$  as Boozer angles, defined in appendix C, and  $B_{\max}$  is the maximum of the magnetic field strength on the surface.

In vacuum, we have  $(\lambda/\mu\rho)_l = (1/\mu\rho)_\psi$ , as can be seen from the expression for the current (2.8) or equivalently by setting  $p'(\psi) = 0$  in the expression for MHS force balance

(3.10). Using that  $B = 1/\mu\rho$  is independent of  $\alpha$ , we integrate this to find

$$\lambda = \frac{1}{B(l, \psi)} \int^l dl' \partial_\psi B(l', \psi) + \frac{f(\psi)}{B(l, \psi)}, \quad (4.7)$$

where  $f$  is the integration constant and is independent of  $\alpha$  because we have  $\lambda_\alpha = 0$ , as in equation (3.9f). We now consider the transformation from  $(l, \alpha, \psi)$  coordinates to  $(\phi, \alpha, \psi)$ , where  $\phi$  is the toroidal Boozer angle. We thus have

$$\left( \frac{\partial}{\partial \psi} \right)_l = \left( \frac{\partial}{\partial \psi} \right)_\phi + \left( \frac{\partial \phi}{\partial \psi} \right)_l \left( \frac{\partial}{\partial \phi} \right)_\psi, \quad (4.8)$$

$$= \left( \frac{\partial}{\partial \psi} \right)_\phi + \left( \frac{1}{G} \int dl' \partial_\psi B(l', \psi) \right) \left( \frac{\partial}{\partial \phi} \right)_\psi. \quad (4.9)$$

The second equality follows from noting that in vacuum, the magnetic field can be written as  $\mathbf{B} = G \nabla \phi$ , where  $G$  is constant. In other words,  $G\phi$  is the magnetic potential for a vacuum magnetic field. Rearranging this expression and using  $\partial_\phi = (G/B)\partial_l$  gives

$$\left( \frac{\partial}{\partial \psi} \right)_\phi = \left( \frac{\partial}{\partial \psi} \right)_l - \lambda \left( \frac{\partial}{\partial l} \right)_\psi, \quad (4.10)$$

where we have absorbed the constant  $f(\psi)$  into the choice of origin between  $l$  and  $\phi$ .

Now, we return to the fact that the current in the  $\partial_\alpha \mathbf{r}$  direction vanishes:  $(\lambda/\mu\rho)_l = (1/\mu\rho)_\psi$ . We combine this with (3.9g) to find

$$\frac{\kappa}{\rho} = (\partial_\psi - \lambda \partial_l) B, \quad (4.11)$$

$$= \left( \frac{\partial B}{\partial \psi} \right)_\phi, \quad (4.12)$$

where we have used equation (4.10) in the second equality. For a foliation of Hasimoto surfaces,  $\kappa/\rho = \gamma(\psi)$ , so we find that

$$B(\phi, \psi) = B_0(\psi) + B_1(\phi) \quad (4.13)$$

where we use the fact that  $B$  depends on only  $\phi$  and  $\psi$ . This arises from equation (3.7b) and is equivalent to quasi-poloidal symmetry in the vacuum case considered here. We find that the magnetic field strength is separable into a radially varying part  $B_0(\psi)$  and a surface-varying part  $B_1(\phi)$ , which is constant across flux surfaces. As an even stronger constraint on the field strength, this satisfies the flat mirror condition (4.6). Technically, for the benefits of a flat mirror to be gained, it is required that  $\partial_\psi B_{00} > 0$  (Velasco *et al.* 2023). However, this can often be achieved by adding a finite plasma pressure, due to the plasma behaving diamagnetically. We have indeed concluded that vacuum foliations of Hasimoto surfaces, which are a subset of QP magnetic fields, are flat mirrors. The optimisation problem sketched in §3.3 can be easily modified to look for Hasimoto surfaces, which then provides a 2D method for investigating flat mirror QP configurations.

Secondly, we derive a differential equation for the magnetic field strength in terms of the surface geometry quantities. In principle, this allows us to express quantities of practical interest, such as the mirror ratio, in terms of the surface geometry. We assume that we have a toroidal Hasimoto surface and that  $(\rho/\kappa)_{l\psi} = 0$ , which is consistent with assuming  $\rho \propto \kappa$  in the neighbourhood of the Hasimoto surface. We do not assume here

that we have vacuum. We first note that equation (3.9h) can be written as

$$\left(\frac{\nu}{\rho}\right)_l = -2\frac{\mu\tau}{\rho}. \quad (4.14)$$

Also, from equations (3.8c), (3.9m), (3.9o), we have

$$\left(\frac{\nu}{\rho}\right)_\alpha = (\partial_\psi - \lambda\partial_l) \ln \frac{\rho}{\kappa} + \left(\frac{4\tau^2}{\kappa} + \kappa - \frac{\rho_{ll}}{\rho\kappa}\right) \frac{1}{\rho B} + \frac{1}{\kappa} \left(\frac{1}{\rho B}\right)_u, \quad (4.15)$$

where we have used  $B = 1/\mu\rho$ , which follows from the definition of the field-line-following coordinate system described in §2. We now equate the  $\alpha$  derivative of equation (4.14) with the  $l$  derivative of equation (4.15)—another compatibility condition. This gives

$$-\left(\frac{2\tau}{B\rho^2}\right)_\alpha = \left[\left(\frac{4\tau^2}{\kappa} + \kappa - \frac{\rho_{ll}}{\rho\kappa}\right) \frac{1}{\rho B} + \frac{1}{\kappa} \left(\frac{1}{\rho B}\right)_u\right]_l, \quad (4.16)$$

where we have used the fact that  $(\rho/\kappa)_l = 0$  and  $(\rho/\kappa)_{l\psi} = 0$ , consistent with field lines obeying the vortex filament equation on the surface and in the neighbourhood of the surface. We now integrate this equation around an integral curve of  $\mathbf{u} = \partial_\alpha \mathbf{r}$ , which is closed in toroidal geometry. Thus, as  $2\tau/B\rho^2$  is single-valued, the left-hand side vanishes and we have

$$\left(\frac{1}{B}\right)_u \oint d\alpha \frac{1}{\rho\kappa} - 2\left(\frac{1}{B}\right)_l \oint d\alpha \frac{\rho_l}{\kappa\rho^2} + \frac{1}{B} \oint d\alpha \frac{1}{\rho\kappa} \left(4\tau^2 + \kappa^2 - \frac{2\rho_{ll}}{\rho} + \frac{2\rho_l^2}{\rho^2}\right) = C, \quad (4.17)$$

where  $C$  is some constant and we have used  $\partial_\alpha B = 0$ . This equation establishes a relationship between the magnitude of the magnetic field and the geometry of the field lines, given a toroidal Hasimoto surface.

In this subsection, we have used  $\kappa/\rho = \gamma(\psi)$  not only on the surface but also in its neighbourhood. In doing so, extra consistency conditions arise by combining equations (3.9m) and (3.9o). We have not considered the consequences of enforcing this consistency.

## 5. Verification on optimised numerical QP magnetic fields

In this section, we present numerically generated vacuum QP magnetic fields, with the primary purpose of corroborating the surface equations. We present two sets of toroidal magnetic field configurations, with specifications detailed in table 1.

The first three magnetic field configurations were produced and optimised for using the DESC code (Dudt & Kolemen 2020). By the nature of the method for calculating the equilibrium field, this equilibrium necessarily has nested flux surfaces. Each configuration was produced by optimising for QP on the boundary (not throughout the whole volume), alongside an aspect ratio and rotational transform target on the boundary, and a vacuum target throughout the volume. The initial condition for the optimisation came from the same class as that in section 3 of Goodman *et al.* (2023).

We also present two magnetic field configurations which were solved for by the SPEC code (Hudson *et al.* 2012). They were optimised for using the adjoint methods developed in Nies *et al.* (2022). These configurations are exactly vacuum throughout the whole volume, which comes at the cost of not necessarily having nested flux surfaces. As with the other set, these configurations were generated by optimising for QP on the boundary, alongside an aspect ratio and rotational transform target. The initial condition for the optimisation was a rotating ellipse with the desired aspect ratio and rotational transform, as predicted by Mercier (1964). In both sets of configurations, the optimisation took place

Configuration	MHS Solver	AR	$\iota$	$R$	NFP
1	DESC	14.12	0.30	0.74	2
2	DESC	11.36	0.11	0.85	5
3	DESC	14.09	0.20	0.51	2
4	SPEC	6.02	0.27	0.97	5
5	SPEC	6.00	0.62	0.97	5

TABLE 1. We present specifications of the five numerical, QP equilibria, including the aspect ratio AR, the rotational transform  $\iota$  on the boundary, the mirror ratio  $R = (\max(B) - \min(B))/(\max(B) + \min(B))$  on the boundary, and the number of field periods, NFP.

in steps, with successive increases to the number of boundary modes (Landreman & Paul 2022).

In the following subsections, we comment on the quality of quasi-poloidal symmetry (§5.1), we detail how the surface equations are verified (§5.2), and then we explain deviations from the surface equations through the appearance of cusps (§5.3), non-zero parallel current (§5.4), and loss of geodesicity (§5.5). Finally, we note the preference for high mirror ratios, double wells, and narrow pinch points in §5.6.

### 5.1. Quality of quasi-poloidal symmetry

We define the QP error on a surface of a configuration as

$$\text{QP error} = \frac{\int_0^{2\pi} d\vartheta \int_0^{2\pi} d\varphi \sqrt{g_{\text{surf}}} \frac{1}{B^3} |\mathbf{B} \times \nabla B \cdot \nabla \psi|}{\int_0^{2\pi} d\vartheta \int_0^{2\pi} d\varphi \sqrt{g_{\text{surf}}}}, \quad (5.1)$$

where  $2\pi\psi$  is the toroidal magnetic flux and  $\int_0^{2\pi} d\vartheta \int_0^{2\pi} d\varphi \sqrt{g_{\text{surf}}} (\dots)$  is an integral over the surface, given that  $(\vartheta, \varphi)$  are the computational poloidal and toroidal angle coordinates (not necessarily straight field-line coordinates) and  $\sqrt{g_{\text{surf}}} = |\partial \mathbf{r} / \partial \vartheta \times \partial \mathbf{r} / \partial \varphi|$  is the surface Jacobian. This QP error is based on the commonly used ‘two-term’ formulation of quasisymmetry (see, e.g., Helander 2014), but there is only one term because we aim for QP configurations which have zero enclosed toroidal current. The QP objective function used during the optimisations was slightly different to this QP error definition and is spelled out in appendix G.

For the five configurations, we present the quality of quasi-poloidal symmetry as a function of the surface in figure 4. We also make the comparison with the magnetic field design for the proposed Quasi-Poloidal Stellarator Experiment (QPS) (Nelson *et al.* 2003; Spong *et al.* 2005). Optimising for QP using standard methods is more difficult than for QA or QH (Landreman & Paul 2022), hence the higher-than-ideal level of QP error. Nonetheless, the DESC configurations represent an improvement over QPS. The difficulty of optimising for QP using standard methods provides additional motivation for the alternative optimisation scheme presented in §3.3.

### 5.2. How the surface equations are tested

The first two surface equations, (3.8a) and (3.8b), are purely geometric and are satisfied by any embedded surface foliated by geodesic field lines. Thus, to verify the first two surface equations, it suffices to ensure that the geodesic curvature is negligible on the boundary surface. As it turns out, this is a direct target for the optimiser as the geodesic

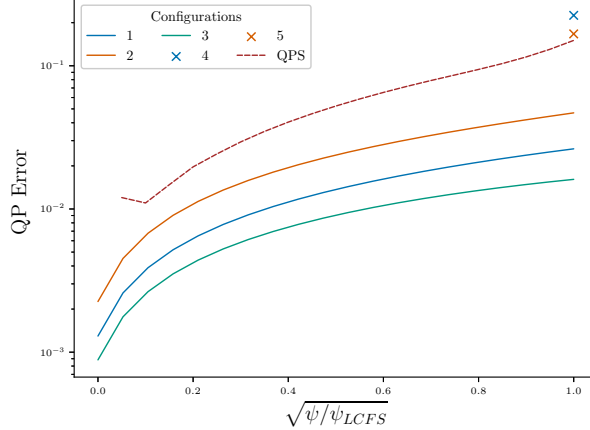


FIGURE 4. The QP error (defined in equation (5.1)) for six different magnetic field configurations as a function of the flux surface. Configurations 1-3 were produced using **DESC** and configurations 4 and 5 were produced using **SPEC** (QP error plotted only on boundary where a flux surface necessarily exists). ‘QPS’ corresponds to the magnetic field design for the Quasi-Poloidal Stellarator ([Nelson et al. 2003](#); [Spong et al. 2005](#)). Configurations 1-3 show an improvement over QPS. Despite QP being only targeted on the boundary, there is a lower level of QP towards the axis.

curvature is proportional to the local QP error on a surface:

$$\frac{1}{B^3} \mathbf{B} \times \nabla B \cdot \nabla \psi = \rho \kappa_g, \quad (5.2)$$

(cf., equation (5.1) and the optimiser objective functions presented in appendix G). That  $\kappa_g \rightarrow 0$  leads to QP was explained in §3.1: a surface with geodesic field lines, zero net enclosed toroidal current, and zero normal current is necessarily QP. Despite being a direct target of the optimiser, deviations from zero geodesic curvature do exist and are significant, as demonstrated in §5.3.

The third surface equation, (3.8c), is assessed directly. For this, we need to interpret  $\kappa$ ,  $\rho$ , and  $\partial_\alpha$  for our numerical equilibria. We take  $\kappa$  to be the normal curvature,  $\kappa_n$ . For calculating  $\rho$ , we use the transformation to Boozer coordinates

$$\theta = \vartheta + \tilde{\lambda} + \iota\omega, \quad (5.3a)$$

$$\phi = \varphi + \omega, \quad (5.3b)$$

where  $\tilde{\lambda}(\vartheta, \varphi)$  gives the transformation to straight field-line coordinates and  $\omega(\vartheta, \varphi)$  gives the transformation from those coordinates to Boozer coordinates. Calculating  $\tilde{\lambda}$  and  $\omega$  from numerical equilibria is standard practice—see [Nies et al. \(2022\)](#) for how this is done for the **SPEC** equilibria without assuming nested flux surfaces. In vacuum, the magnetic field can be written as  $\mathbf{B} = G \nabla(\omega + \varphi)$ , where  $G$  is constant. Given the surface Jacobian  $\sqrt{g}_{\text{surf}} = |\partial \mathbf{r} / \partial \vartheta \times \partial \mathbf{r} / \partial \varphi|$ , we then take  $\rho$  to be

$$\rho = \frac{\sqrt{g}_{\text{surf}} B}{G \left| (1 + \omega_\varphi) \left( 1 + \tilde{\lambda}_\vartheta \right) - \omega_\vartheta \left( \tilde{\lambda}_\varphi - \iota \right) \right|}, \quad (5.4)$$

where  $\iota$  is the rotational transform. This agrees with the theoretical definition of  $\rho$  when  $\kappa_g = 0$ , as shown in appendix H.

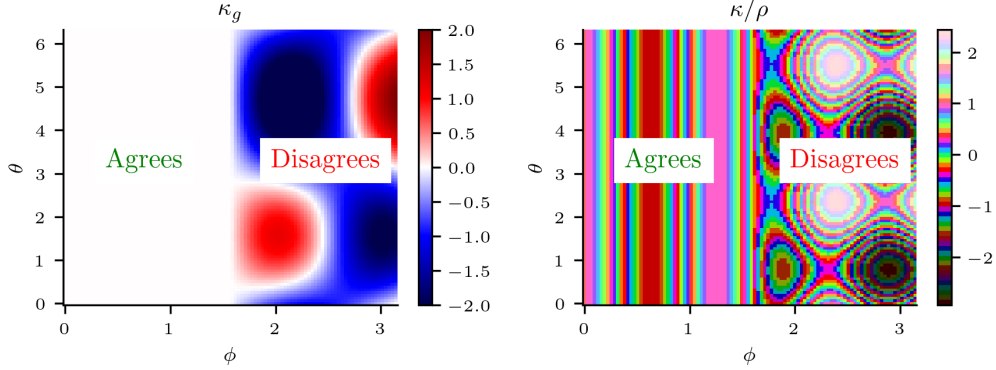


FIGURE 5. A schematic example of what it looks like for the surface equations to be verified or falsified on a flux surface. For  $\phi < \pi/2$ , there is agreement with the surface equations, since the geodesic curvature is zero and  $\kappa/\rho$  only depends on  $\phi$ . For  $\phi > \pi/2$ , there is disagreement as the geodesic curvature is non-zero and  $\kappa/\rho$  does not have vertical contours.

Finally, we note that

$$\left( \frac{\partial}{\partial \theta} \right)_\phi = 0 \iff \left( \frac{\partial}{\partial \alpha} \right)_l = 0, \quad (5.5)$$

so the third surface equation is verified if and only if  $\kappa/\rho$  depends only on  $\phi$ . In figure 5, we illustrate what the plots of  $\kappa_g$  and  $\kappa/\rho$  on the boundary should look like for the surface equations to be verified.

### 5.3. The appearance of cusps

In this subsection, we consider the first DESC magnetic field configuration. For this configuration, the vacuum target was essentially achieved. In figure 6a), we see that  $\kappa/\rho$  varies primarily horizontally in agreement with the third surface equation, except for regions of sharp vertical change around  $\theta \approx 1$  and  $\theta \approx 4.5$  for  $\phi \in (0.75, 2.5)$ . This does not falsify the third surface equation because these are precisely the regions where the geodesic curvature deviates significantly from zero, as can be seen from figure 6b). After all, zero geodesic curvature was an assumption behind the derivation of the surface equations.

In fact, we can understand these deviations from the surface equations through the surface equations themselves. The curvature  $\kappa$  is negative whenever the field line principal normal is opposed to the surface normal. Based on intuition from tokamaks, the inboard and outboard sides of the torus typically have opposite signs of  $\kappa$ . However, the third surface equation tells us that  $\kappa/\rho$  should be constant on poloidal loops, so  $\kappa$  should not be able to change sign, since  $\rho > 0$ . The optimiser rectifies this difficulty by isolating the regions where  $\kappa$  changes sign to thin cusps, with  $\kappa/\rho$  independent of  $\theta$  only away from these cusps. The cusps are visible in figure 6c) at  $\phi \approx 0.5\pi$ , which also happens to be where the surface ‘curves around’.

We note that the cusps also appear to follow the field lines. This can be understood through MHS force balance. As the field is vacuum, it is necessarily force-free, so the tension force from the field lines can only be balanced by magnetic pressure. The magnetic pressure can only grow so large given the limited field strength variation, so the magnetic tension force has to be minimised by not having field lines go across the cusp.

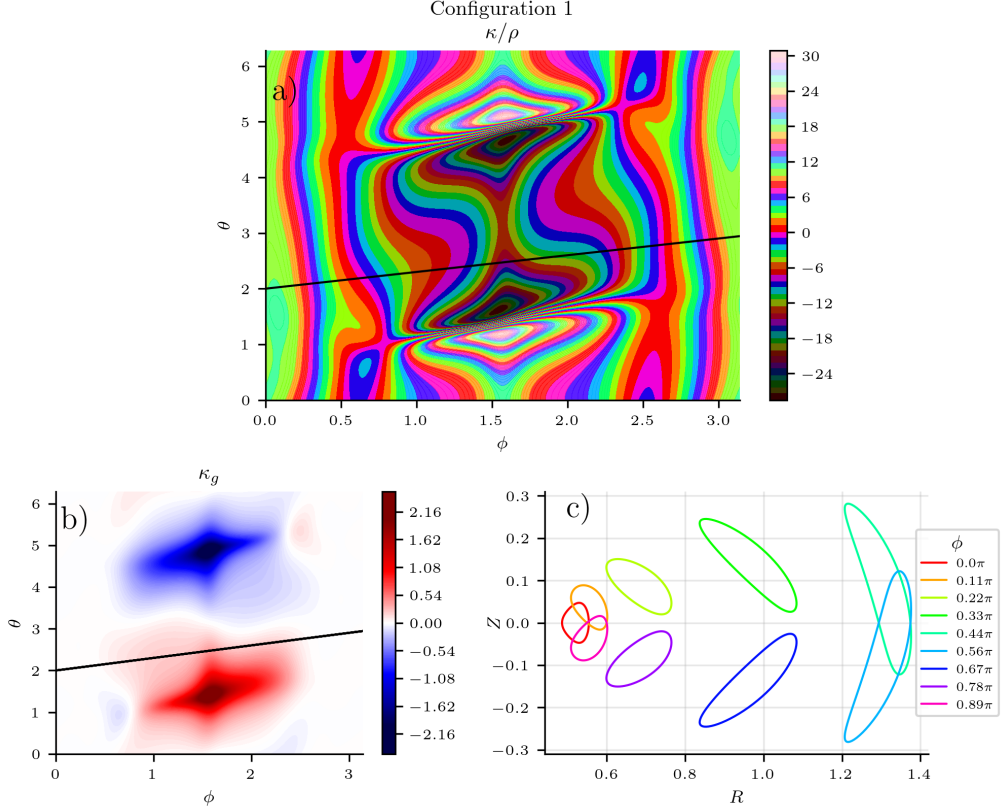


FIGURE 6. We plot quantities for the first DESC configuration: a)  $\kappa/\rho$  and b) the geodesic curvature  $\kappa_g$ , both on the boundary surface as a function of Boozer angles, and c) toroidal cross-sections of the boundary flux surface. Lengths are measured with respect to the average major radius. The black line in a) and b) is a field line. We see decent agreement with the third surface equation, except the regions with large geodesic curvature (i.e., where QP-breaking is significant).

#### 5.4. The effect of parallel current

We now consider the second DESC magnetic field configuration. In figure 7a), we observe noticeable departure from the third surface equation, since the contours are largely not close to vertical. There are two related reasons for this.

Firstly, consider the region  $\phi \in (0.4, 0.8)$ . This region of the surface is similar to the configuration considered in the last subsection: there are approximately straight contours separated by ‘cusps’, which is where the geodesic curvature is largest (see figure 7b)). The geodesic curvature deviates somewhat from zero even away from these cusps, which explains why the vertical contours are slightly curved and angled. As in the last subsection, we can explain the cusps by the fact that  $\kappa$  typically has to change sign from the inboard to the outboard side, in contradiction with the third surface equation.

Now, consider the remaining portion of the surface:  $\phi \in (0, 0.4)$  and  $\phi \in (0.8, 2\pi/5)$ . The contours are not vertical here at all, despite the geodesic curvature being small. Here, it is another assumption of the surface equations which breaks down: the parallel current is non-zero. Zero current density was a target for the optimiser but was not sufficiently attained everywhere in this configuration.

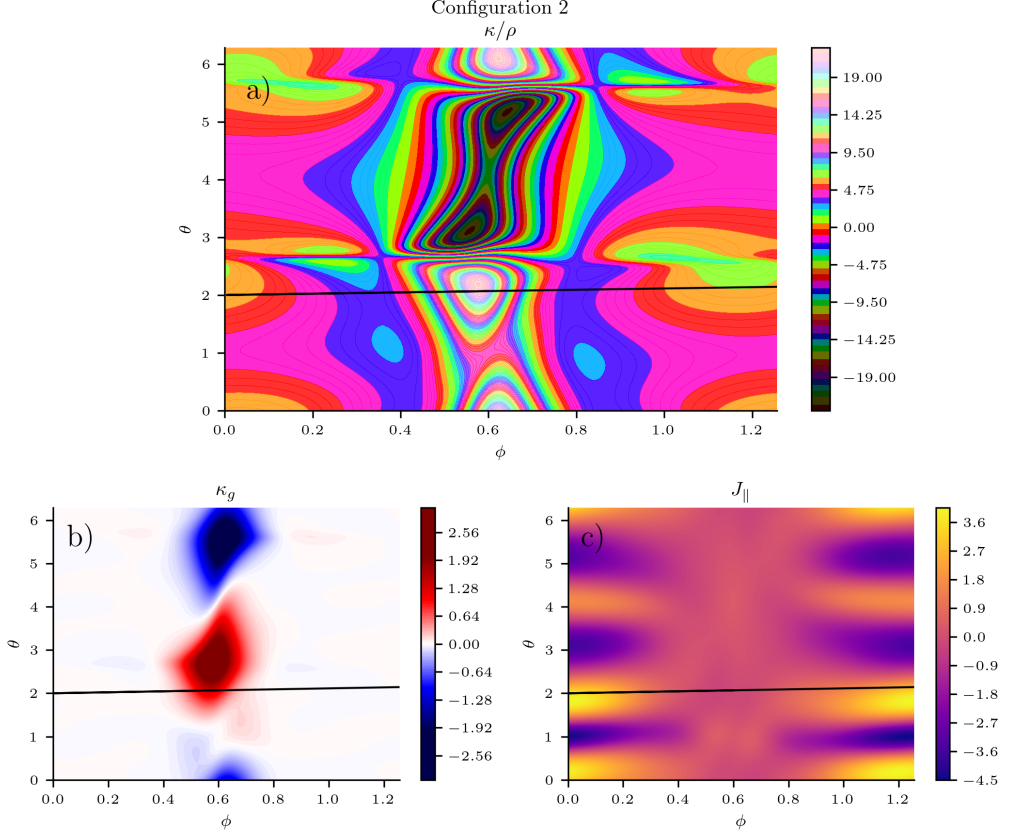


FIGURE 7. For the second DESC configuration: a)  $\kappa/\rho$ , b) the geodesic curvature  $\kappa_g$ , and c) the parallel current  $J_{\parallel}$ . All quantities are plotted on the boundary surface as a function of Boozer angles. Lengths are measured with respect to the average major radius and the current is normalised by the mean magnetic field on the boundary. There are two related reasons for deviations from the third surface equation: areas of high geodesic curvature and large parallel current.

Even without considering the vacuum target, having non-zero parallel current is somewhat unexpected. This is because of the theoretical result presented at the end of appendix C: assuming QP, force-balance, and zero net toroidal current, the parallel current should vanish pointwise. The magnetic field configuration presented in figure 7 does indeed have zero net toroidal current and is force-balanced (as current perpendicular to the field lines is indeed negligible). Moreover, in the relevant region where parallel current is non-zero, the geodesic curvature is small, which corresponds to the local QP error being small (see §5.1). However, it is the local QP error in a separate region ( $\phi \in (0.4, 0.8)$ ), where there are cusps and high geodesic curvature, which allows for non-zero parallel current elsewhere on the surface. This is a non-local effect.

### 5.5. When are field lines sufficiently geodesic?

In this subsection, we use the third DESC magnetic field configuration to point out that the third surface equation is satisfied (locally) only if the field lines are sufficiently geodesic, in the sense that the geodesic curvature should be much smaller than the normal curvature.

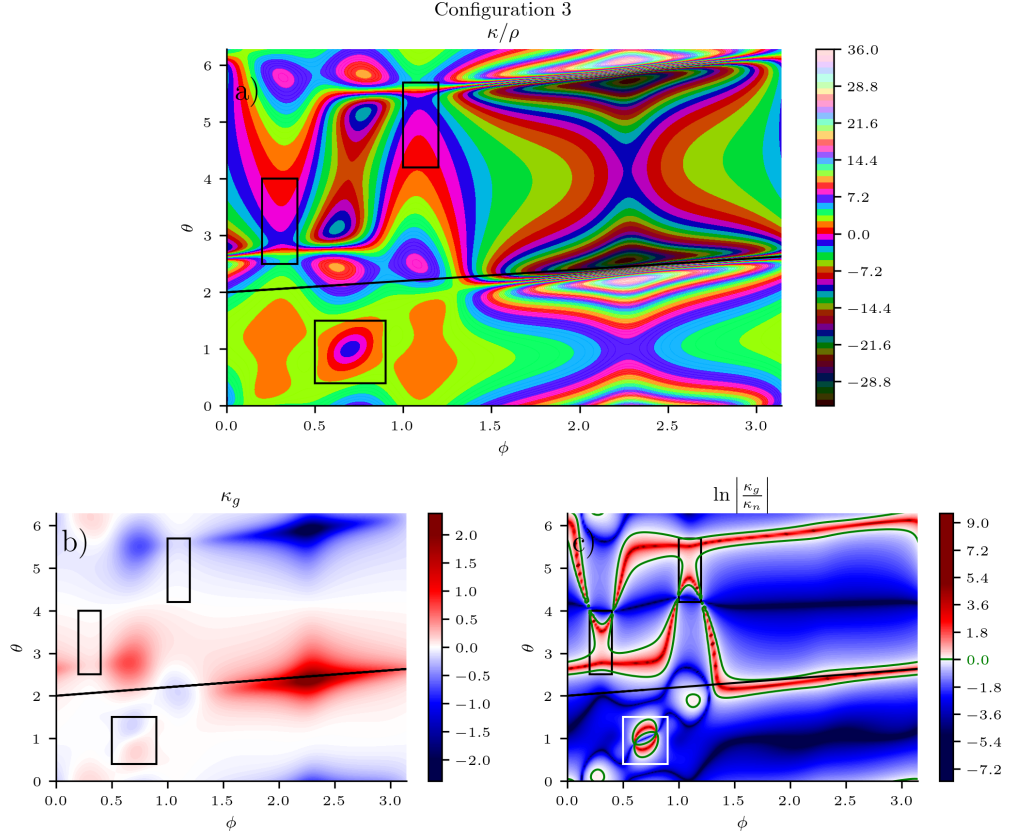


FIGURE 8. For the boundary surface of the third DESC configuration: a)  $\kappa/\rho$ , b) the geodesic curvature  $\kappa_g$ , and c) the logarithm of the geodesic curvature divided by normal curvature  $\kappa_n$ . For the third surface equation to be true, the geodesic curvature should be small compared to the normal curvature, which is not the case within the overlaid black/white rectangles.

We consider two different parts of the boundary surface of this configuration. The region  $\phi \in (1.3, \pi)$  is similar to the central region of the first configuration considered in §5.3: the third surface equation is violated on field-line-following cusps (see figure 8a)), which is where the geodesic curvature (and thus QP error) is large, as per figure 8b). Away from these cusps, the contours of  $\kappa/\rho$  are nearly vertical.

We now consider the region  $\phi \in (0, 1.3)$ , where the magnetic field strength is largest. Apart from distinct blobs at  $(\phi, \theta) \approx (0.7, 3)$  and at  $(\phi, \theta) \approx (0.7, 5.5)$ , the geodesic curvature is relatively small in an absolute sense, as per figure 8b). These blobs can also be thought of as cusps, and also represent areas where the third surface equation does not hold (contours of  $\kappa/\rho$  are not vertical). However, even away from these blobs, the contours are not close to vertical, particularly in the regions outlined by the black rectangles in figure 8a). As seen in figure 8b), the geodesic curvature is small in these regions, in an absolute sense. However, as seen from figure 8c), the geodesic curvature is much larger than the normal curvature in these regions, so the field lines cannot be considered geodesics in these regions. Given that the geodesicity of field lines was an assumption of the surface equations, deviation from the third surface equation is to be expected in these regions.

Given that the normal curvature does not directly enter into the definition of QP error

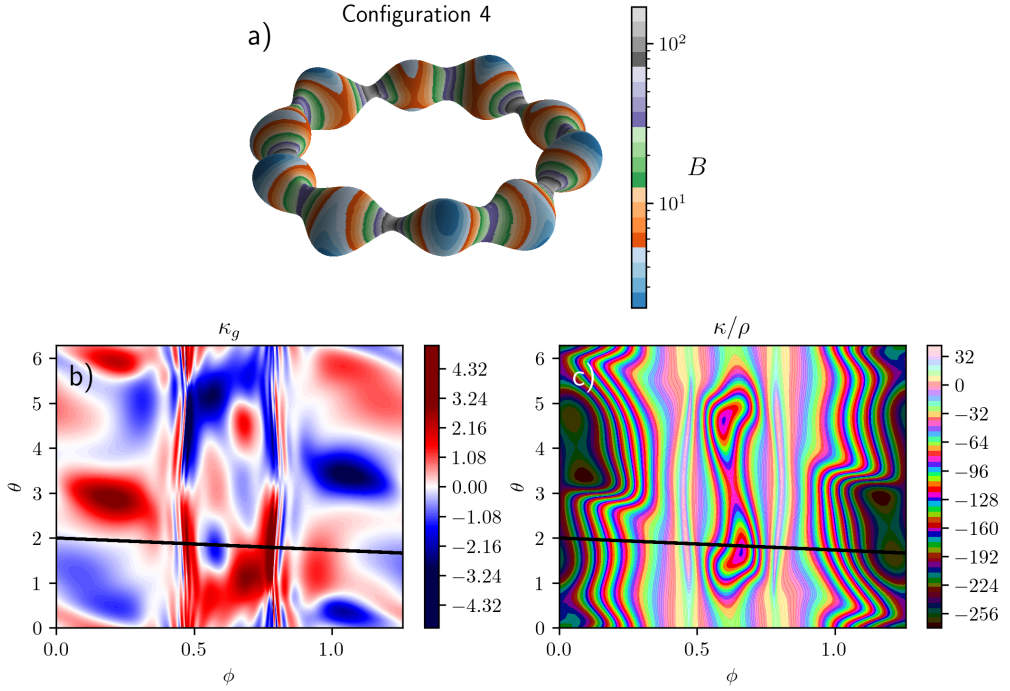


FIGURE 9. For the first SPEC configuration, we plot a) the boundary surface in real space, b)  $\kappa_g$  on the boundary, and c)  $\kappa/\rho$  on the boundary. Lengths are measured in terms of the average major radius and the black line on b) and c) is a field line. We observe a very large mirror ratio, narrow pinch points, and double wells.

(cf., equations (5.1) and (5.2)), this observation suggests that it is possible to have a surface of high QP quality without having that surface conform to the surface equations, as long as the normal curvature is sufficiently small. This would be most readily achieved for a high aspect ratio stellarator, where it is conceivable for normal curvature to remain small everywhere. However, this would constitute a Pyrrhic victory. As discussed in §1, many practical advantages stem from the radial drift of the guiding centres being much smaller than the poloidal drift. If geodesic curvature is larger than normal curvature, the radial drift is larger than the poloidal drift, so one loses these practical advantages.

### 5.6. High mirror ratios and narrow pinch points

In this subsection, we focus on the two SPEC equilibria. By construction, these are vacuum equilibria. Thus, we need not worry about non-zero currents undermining the surface equations, as was the case in §5.4. This comes at the cost of not necessarily having nested flux surfaces, which permits pathologically narrow pinch points in the boundary surface, seen in figures 9a) and 10a).

In figures 9 and 10, we plot  $\kappa/\rho$  and  $\kappa_g$  on the boundary surface. Due to the regions of large geodesic curvature, there are deviations from the third surface equation as the contours of  $\kappa/\rho$  are not vertical. There are vertical contours in select regions, particularly in figure 9c).

For completeness, we note an additional potential reason for deviation from the third surface equation. In deriving the surface equations, we assumed not only that the

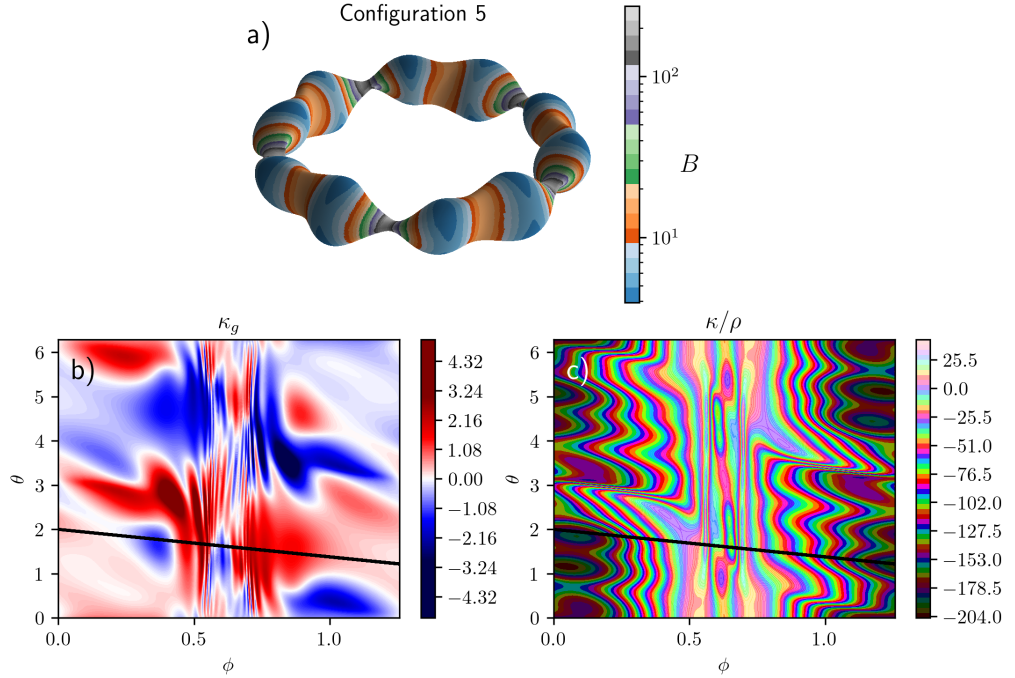


FIGURE 10. For the second SPEC configuration, we plot a) the boundary surface in real space, b)  $\kappa_g$  on the boundary, and c)  $\kappa/\rho$  on the boundary. Lengths are measured in terms of the average major radius and the black line on b) and c) is a field line. We observe a very large mirror ratio, narrow pinch points, and double wells.

field lines are geodesics on the flux surface, but also that field lines are geodesics in the neighbourhood of the surface (see equation (3.7a) and surrounding discussion). In other words, we assumed QP in the neighbourhood of the surface. Thus, in these SPEC configurations, non-geodesic field lines adjacent to the flux surface can contribute to deviations of the third surface equation. This differs from the DESC configurations, where imposing nested flux surfaces naturally leads to a high level of QP on neighbouring surfaces.

One can observe in figures 9a) and 10a) that the SPEC configurations resemble a system of ‘linked magnetic mirrors’. This observation is consistent with the surface equations, since magnetic mirrors are solutions to the surface equations with poloidally-closing orthogonals to the field lines.

We also observe narrow pinch points and extremely high mirror ratios in the SPEC configurations, as seen in figures 9a) and 10a). Even with a prescribed number of field periods, the optimiser tended to ‘double’ the field periods in these configurations. In other words, the optimisation would occasionally produce a ‘double well’, with two minima of the magnetic field strength within a single field period.

Based on the similarity with magnetic mirrors, we can explain the appearance of narrow pinch points, high mirror ratios, and double wells through the surface equations. As it turns out, magnetic mirrors with narrow pinch points can more readily bend around (as is necessary to form a toroidal surface) and generate a non-zero rotational transform. This claim is justified in appendix I, where we perturb surfaces of revolution through

the surface equations, form an eigenvalue problem (given periodic boundary conditions), and show that the density of eigenvalues increases given a narrow pinch point.

In addition to this mathematical argument, we can understand physically why narrow pinch points assist in having non-zero rotational transform. The field lines are geodesics, which are paths of inertial motion on the surface. Akin to a ballerina pulling their arms in to spin faster, a narrower pinch point will assist the geodesic field lines ‘spinning around’ the surface, generating a rotational transform. This physical interpretation does not extend to explaining why narrower pinch points also assist in the surface being able to ‘bend around’.

To summarise this section, we have found that the surface equations are verified in numerically optimised QP equilibria on local patches of the surface where the local QP error and local parallel currents are sufficiently small. The local QP error is proportional to the geodesic curvature, and we found that for the surface equations to be approximately satisfied, the geodesic curvature must be much smaller than the normal curvature. We observe a tendency for cusps to form on the surface, corresponding to areas of high geodesic curvature and deviations from the third surface equation. These cusps appear because of the optimiser’s predicament: the third surface equation implies that  $\kappa$  has a constant sign along the poloidal loops, but typical toroidal surfaces have  $\kappa$  switching sign between the inboard and outboard sides. Finally, for QP surfaces that resemble linked magnetic mirrors, we found that narrow pinch points and high mirror ratios were consistent with the surface equations.

## 6. Conclusions

The main result of this paper is the surface equations (3.8), which represent a striking reduction of the problem of finding QP flux surfaces, as well as desirable asymmetric magnetic-mirror surfaces. Rather than solving the full 3D problem of finding a surface as well as neighbouring field lines, it suffices to solve the 2D problem of the surface equations. The surface equations were verified against numerically optimised QP equilibria in §5, where deviations from the surface equations correlated with local QP error (i.e., non-zero geodesic curvature) or significant parallel currents. The surface equations also provide a theoretical framework for understanding QP solutions in lieu of a near-axis expansion. For instance, we qualitatively explained why numerically optimised QP stellarators tend to have cusps: the optimiser attempts to reconcile the requirement that  $\kappa/\rho$  remain constant on poloidal loops with the fact that  $\kappa$  generally switches sign between the inboard and outboard sides of a toroidal surface. In addition, we identified two basic classes of solutions to the surface equations: generalised helicoids (including magnetic mirrors) and Hasimoto surfaces, which are surfaces traced out by a vortex filament. We observed that some numerical QP equilibria resemble linked magnetic mirrors and used this to explain the appearance of narrow pinch points and high mirror ratios. For toroidal Hasimoto surfaces, we developed a theory for the field strength, demonstrating that such surfaces in vacuum are flat mirrors; such configurations are of particular interest because they exhibit robust confinement of fast ions and small radial transport of energy.

We outline directions for future work. The simplified, efficient optimisation problem, sketched out in §3.3, remains to be numerically implemented. This would allow for the production of a database of QP flux surfaces from which trends could be analysed. Other work (Haque *et al.* 2026) demonstrates that a high level of QP is possible, with some verification of the attractive physical benefits that come with QP, such as improved fast ion confinement. Further investigation is needed to verify some other attractive features of QP, such as turbulence suppression from poloidal shearing flows. Finally, one could

use the surface equations in designing a magnetic mirror that is MHD stable and has good radial, collisionless particle confinement.

This research was supported by a grant from the Simons Foundation/SFARI (560651, AB) and the Department of Energy Award No. DE-SC0024548 (until March 31, 2025).

## Appendix A. Impossibility of exact QP near the magnetic axis

We reproduce the proof that quasi-poloidal symmetry is impossible near the magnetic axis (Landreman 2011; Helander 2014).

The curvature vector  $\kappa = \kappa \hat{n}$  can be written as

$$\kappa = -\hat{t} \times (\nabla \times \hat{t}), \quad (\text{A } 1)$$

$$= -\hat{t} \times \left( \nabla \frac{1}{B} \times \hat{t} \right) - \frac{\hat{t}}{B} \times \mathbf{J}, \quad (\text{A } 2)$$

$$= \frac{\nabla p}{B^2} + \frac{\nabla_{\perp} B}{B}, \quad (\text{A } 3)$$

where we have used MHS force balance (3.1) and  $\nabla_{\perp} = \nabla - \hat{t} \hat{t} \cdot \nabla$ . Close to the axis,  $\nabla \psi \rightarrow 0$ . Thus, as  $\nabla p \propto \nabla \psi$ , we also have  $\nabla p \rightarrow 0$ . In Boozer (1981) coordinates  $(\theta, \phi)$ , the magnetic field can be written as  $\mathbf{B} = G(\psi) \nabla \phi + I(\psi) \nabla \theta + \beta(\psi, \theta, \phi) \nabla \psi$ , where  $2\pi\psi$  is the toroidal magnetic flux and  $2\pi I(\psi)$  is the net toroidal current enclosed by the flux surface. Assuming the current parallel to the magnetic axis is not singular, we take  $I \rightarrow 0$  as  $\psi \rightarrow 0$ , where  $\psi = 0$  on the axis. We also assume  $\beta$  stays bounded for  $\psi \rightarrow 0$ . Thus, close to the axis,  $\mathbf{B} = G(0) \nabla \phi$ . So, we have

$$|\kappa| \propto \frac{\partial B}{\partial \theta}. \quad (\text{A } 4)$$

To form a closed loop, the axis has to curve somewhere, so at some point along the axis,  $|\kappa| \neq 0$ . Thus, somewhere  $\partial_{\theta} B \neq 0$ , contradicting quasi-poloidal symmetry, which requires  $B = B(\psi, \phi)$  by definition. There is a stronger version of this argument that shows QP is not possible close to the axis without invoking MHS force balance (Rodriguez 2022).

*Prima facie*, this proof seems to dismiss quasi-poloidal symmetry as a possibility. However, a few provisos are in order. Firstly, this proof does not imply that QP cannot be achieved away from the axis, where having good QP is arguably more important. Notably, in a small aspect ratio stellarator, more of the stellarator volume will be away from the near-axis limit. Secondly, in the opposite limit of large aspect ratio, the curvature of the axis  $|\kappa|$  is small, so the level of QP-breaking can also be made small, as seen in equation (A 4). Thus, this proof has limited consequences for both small aspect ratio and large aspect ratio stellarators.

For completeness, we also list two technical ways to circumvent the proof. Firstly, one could have a singular current on the axis so that  $I(\psi = 0) \neq 0$ . Secondly, the magnetic field on the axis can be made to vanish. These are not desirable possibilities for magnetic confinement.

## Appendix B. Equivalence of moving frame and Riemann curvature conditions

Though we introduced  $\mathbf{K}$ ,  $\chi$ , and  $\sigma$  in §2, physically we have just imposed the flatness of Euclidean space on the metric components, given by  $\rho, \eta, \lambda, \mu$ , and  $\nu$ . The Riemannian

curvature tensor is defined as

$$\mathcal{R}(X, Y)Z = \nabla_X \nabla_Y Z - \nabla_Y \nabla_X Z - \nabla_{[X, Y]} Z, \quad (\text{B1})$$

where  $\nabla$  denotes the covariant derivative,  $[X, Y] = (X^j \partial_j Y^i - Y^j \partial_j X^i) \partial_i$  is the Lie bracket, and  $X, Y, Z$  are arbitrary vector fields (Riemann & Weber 1953). As an example, we take  $X = \partial/\partial l$ ,  $Y = \partial/\partial \alpha$ , and  $Z = \mathbf{e}_i$ , where we have defined  $(\mathbf{e}_1, \mathbf{e}_2, \mathbf{e}_3) = (\hat{\mathbf{t}}, \hat{\mathbf{n}}, \hat{\mathbf{b}})$ . Then, using the fact that the Lie bracket of coordinate fields vanishes, we have

$$\mathcal{R} \left( \frac{\partial}{\partial l}, \frac{\partial}{\partial \alpha} \right) \mathbf{e}_i = \left( \frac{\partial \chi_{ij}}{\partial l} - \frac{\partial K_{ij}}{\partial \alpha} + \chi_{ik} K_{kj} - K_{ik} \chi_{kj} \right) \mathbf{e}_j, \quad (\text{B2})$$

where we have used the skew-symmetric matrix versions of  $\mathbf{K}$  and  $\chi$ , i.e.,  $K_{ij} = \epsilon_{ijk} K_k$ . This can be repeated for other combinations of the coordinate fields. Then, by equations (2.4), we conclude that  $R = 0$ , as required. Equations (2.5), (2.6), and (2.7) can be interpreted as definitions of  $\mathbf{K}$ ,  $\chi$ , and  $\sigma$ , reducing the equations (2.4) to flatness conditions on the metric.

## Appendix C. Relation between $(l, \alpha)$ and Boozer coordinates

In this appendix, we detail the transformation between the  $(l, \alpha)$  coordinates used in this paper and Boozer coordinates  $(\theta, \phi)$ , where  $\theta$  is the poloidal angle and  $\phi$  is the toroidal angle. We do this for the particular case of QP symmetry with  $2\pi I(\psi) = 0$ , where  $I$  is the enclosed toroidal current for a flux surface with enclosed toroidal flux  $2\pi\psi$ . Due to  $I = 0$ ,  $\mathbf{B} = G(\psi) \nabla \phi + \beta(\psi, \theta, \phi) \nabla \psi$  and the Jacobian in this coordinate system is  $G(\psi)/B^2$ . QP is then expressed as  $B = B(\psi, \phi)$  (see, e.g., Helander 2014).

It can be shown that  $\mathbf{u} = (\partial \mathbf{r} / \partial \theta)_{\phi, \psi}$  satisfies (3.4) for QP, where  $B = B(\psi, \phi)$ . It is then clear that  $\mathbf{u} \cdot \mathbf{B} = 0$ . The arc length along the field line, with a particular choice of origin, is given by

$$l = \int_0^\phi d\phi' \frac{G(\psi)}{B(\psi, \phi')} \cdot \quad (\text{C1})$$

We also take  $\alpha = \theta - \iota\phi$ . Since  $l = l(\psi, \phi)$ , we then see that  $\mathbf{u} = (\partial \mathbf{r} / \partial \alpha)_{l, \psi}$ , as required.

Also, as a corollary, we see that the length of a field line segment from  $\phi = 0$  to  $\phi = 2\pi$  is independent of the field line. This length is  $L$ , as defined in §4.

Furthermore, we show why, given MHS force balance and  $I = 0$ , the parallel current on the surface is zero. Under MHS force balance,  $\beta$  has the same symmetry as the magnetic field strength (see, e.g., Rodriguez 2022). So,

$$\nabla \times \mathbf{B} = \left( \frac{dG}{d\psi} - \frac{\partial \beta}{\partial \phi} \right) \nabla \psi \times \nabla \phi \propto \frac{\partial \mathbf{r}}{\partial \theta}. \quad (\text{C2})$$

Therefore,  $\mathbf{J}$  is perpendicular to  $\mathbf{B}$ . This provides further support for why QP surfaces are natural extensions of LQP surfaces.

## Appendix D. Derivation of the surface equations

In this appendix, we explicitly derive the surface equations (3.8) from the relevant equations for a single LQP flux surface, as laid out in §3.2. We also derive equations (3.9), which are not overdetermined and accompany the surface equations in describing an LQP surface with all its relevant qualities.

To summarise the goal of this derivation, we desire  $\lambda, \mu, \nu, \sigma, \mathbf{K}, \chi, \rho, \eta, \mathbf{K}_\psi, \chi_\psi, \rho_\psi$ , and  $\eta_\psi$  at fixed  $\psi = \psi_0$  as functions of  $(l, \alpha)$  that solve equations (2.4), (2.6), (2.7) at

fixed  $\psi = \psi_0$  and equations (2.5) for  $\psi = \psi_0 + \delta\psi$  (the ‘geometric’ constraints), as well as equations (3.7) (the ‘physical’ constraints). Obtaining a general, analytical solution to these equations is not feasible. Instead, in this appendix, we algebraically reduce these equations to equations (3.8) and (3.9). This reduction allows us to make claims about the surface equations being decoupled and complete, which are expressed in §3.2. In this appendix, variables are taken as functions of  $(l, \alpha)$  at some fixed  $\psi$  corresponding to the surface.

From equations (2.5a), (3.7a), and (3.7c), we have

$$K_2 = 0, \quad K_{2\psi} = 0, \quad (\text{D } 1)$$

noting that equations (2.5) apply at  $\psi_0$  and at  $\psi_0 + \delta\psi$  for infinitesimal  $\delta\psi$ . Similarly, equation (2.5b) gives

$$\chi_3 = \rho\tau, \quad \chi_{3\psi} = (\rho\tau)_\psi, \quad (\text{D } 2)$$

and equation (2.5c) gives

$$\chi_2 = \rho_l, \quad \chi_{2\psi} = \rho_{l\psi}. \quad (\text{D } 3)$$

The second component of equation (2.4a) gives

$$\chi_1 = -\frac{\rho_{ll} - \rho\tau^2}{\kappa}. \quad (\text{D } 4)$$

Though equations (2.4) hold at fixed  $\psi = \psi_0$ , the  $\psi$  derivative of equation (2.4a) is satisfied automatically by equations (2.4b) and (2.4c). Thus, we also have

$$\chi_{1\psi} = -\left(\frac{\rho_{ll} - \rho\tau^2}{\kappa}\right)_\psi. \quad (\text{D } 5)$$

The first component of equation (2.4a) gives, after using the above expressions for  $\chi$ , the second surface equation (3.8b), repeated here for convenience,

$$\tau_\alpha = \rho_l\kappa + \left(\frac{\rho_{ll} - \rho\tau^2}{\kappa}\right)_l, \quad (\text{D } 6)$$

and similarly the third component of (2.4a) gives the first surface equation (3.8a), also repeated here,

$$\kappa_\alpha = -2\rho_l\tau - \rho\tau_l. \quad (\text{D } 7)$$

By the same reasoning that led to equation (D5), we also have the  $\psi$  derivatives of equations (D6) and (D7). But these equations are automatically satisfied due to equations (2.4), so we do not write this explicitly. In other words, this result follows from our expressions for  $\partial_\psi(\rho, \kappa, \tau)$  that we derive below.

Now, equation (2.6a) gives  $\lambda_l = \mu\kappa$ . We take the  $\alpha$  derivative of this and use equations (3.7b) and (3.7c) to get the third surface equation,

$$\left(\frac{\kappa}{\rho}\right)_\alpha = 0. \quad (\text{D } 8)$$

Directly from (3.7b), we take  $\mu$  as a solution to

$$\mu_\alpha = -\frac{\rho_\alpha}{\rho}\mu. \quad (\text{D } 9)$$

Similarly, we take  $\lambda$  as a solution to the compatible differential equations

$$\lambda_\alpha = 0, \quad \lambda_l = \kappa\mu. \quad (\text{D } 10)$$

We now solve equation (2.6b) for  $\sigma_3$ , which gives

$$\sigma_3 = \tau\nu - \kappa\lambda - \mu_l, \quad (\text{D } 11)$$

and similarly, we solve equation (2.6c) for  $\sigma_2$ ,

$$\sigma_2 = \nu_l + \tau\mu. \quad (\text{D } 12)$$

Substituting this solution for  $\sigma_2$  into equation (2.7a) and using the fact that the parallel current vanishes (equation (3.7c)), we obtain

$$\nu_l = \frac{\rho_l}{\rho}\nu - 2\tau\mu. \quad (\text{D } 13)$$

We take  $\nu$  to be a solution to this differential equation.

We still have to satisfy equations (2.7b), (2.7c), (2.4b), and (2.4c).

We solve equation (2.7b) for  $\sigma_1$ ,

$$\sigma_1 = -\frac{\rho_\alpha}{\rho^2}\mu - \tau\lambda - \frac{\rho_{ll} - \rho\tau^2}{\kappa}\frac{\nu}{\rho}, \quad (\text{D } 14)$$

where we have substituted for  $\sigma_3$  and used equation (D 9).

We solve equation (2.7c) for  $\rho_\psi$ ,

$$\rho_\psi = \nu_\alpha + \rho_l\lambda + \frac{\rho_{ll} - \rho\tau^2}{\kappa}\mu, \quad (\text{D } 15)$$

where we have substituted for  $\chi$  and  $\sigma$ .

We solve the first component of equation (2.4b) for  $\tau_\psi$ , which, after using the surface equations, reduces to

$$\tau_\psi = \frac{\tau_\alpha}{\rho}\nu + \tau_l\lambda + \frac{\rho_\alpha}{\rho^2}\mu_l + \left( \left( \frac{\rho_\alpha}{\rho^2} \right)_l - 2\frac{\tau}{\rho}\frac{\rho_{ll} - \rho\tau^2}{\kappa} \right)\mu. \quad (\text{D } 16)$$

Now, using the results we already have, we can in fact *derive* the second component of equation (2.4b). In particular, it follows from equations (D 1), (D 11), (D 13), (D 14), and the surface equations (D 6), (D 7), and (D 8). Thus, equation (2.4b) gives no additional constraints.

We solve the third component of equation (2.4b) for  $\kappa_\psi$ , which gives, after using equations (D 10) and (D 13), as well as the solutions for  $\sigma$ ,

$$\kappa_\psi = \mu_{ll} + (\kappa^2 + 3\tau^2)\mu + \kappa_l\lambda + \frac{\kappa_\alpha}{\rho}\nu. \quad (\text{D } 17)$$

Now we consider the first component of equation (2.4c). For the first component of equation (2.4c), we substitute the solutions for  $\sigma$  and  $\chi$ , as well as for  $\chi_{1\psi}$  from equation (D 5). In the substituted expression for  $\chi_{1\psi}$ , we further substitute the solutions for  $\rho_\psi$ ,  $\kappa_\psi$ , and  $\tau_\psi$ . In this way, it is verified (after much algebra) that the first component of equation (2.4c) is automatically satisfied; i.e., it can be derived from the results we already have and does not impose any further constraints. We can follow a similar process for the other two components of equation (2.4c) and, remarkably, we also find that these equations can be derived from the results we already have.

Thus, we have successfully shown that the relevant equations and variables for defining an LQP flux surface (as laid out in §2 and in equations (3.7)) reduce to the surface equations and the associated system of equations (3.9).

It is instructive to compare this calculation with that of Schief (2003). Our case turns out to be more tractable due to some fortunate cancellations. Namely,  $\mu$  and  $\nu$  are

given as the solutions to individual differential equations (equations (3.9b) and (3.9i)) so there is no overdetermination in these variables and there are therefore no additional compatibility constraints. Remarkably, terms involving  $\mu_l$ ,  $\mu_u$ , and  $\nu_\alpha$  cancel.

## Appendix E. Relationship to the results and language of classical differential geometry

In this appendix, we detail the relationship between the surface equations and some classical results of differential geometry.

We note that equations (3.8a) and (3.8b) came directly from the first two components of equation (2.4a), after substituting for  $\chi$ . Thus, they are purely geometric and satisfied by any embedded surface, written in geodesic coordinates. These two equations are known as the Codazzi-Mainardi equations (Depman 1952; Mainardi 1856; Codazzi 1868).

Given the surface quantities  $(\rho, \kappa, \tau)$ , we can, in principle, reconstruct the surface. This reconstruction is involved, as it requires integrating equations (2.3a) and (2.3b) and further integrating  $\mathbf{r}_l = \hat{\mathbf{t}}$  and  $\mathbf{r}_\alpha = \rho \hat{\mathbf{b}}$ . Some geometric features of the surface are more easily calculated. The differential invariants of the surface are the Gaussian and mean curvature. By Gauss' (1828) *Theorema Egregium*, the Gaussian curvature is

$$K = -\frac{\rho_{ll}}{\rho}. \quad (\text{E1})$$

The mean curvature is

$$H = \kappa - \frac{1}{\rho} \frac{\rho_{ll} - \rho\tau^2}{\kappa}. \quad (\text{E2})$$

In the language of classical differential geometry (see, e.g., Eisenhart 2013), the first fundamental form (also known as the metric or the line element) is

$$\mathbf{I} = d\mathbf{r} \cdot d\mathbf{r}|_{\psi=\psi_0} = dl^2 + \rho^2 d\alpha^2. \quad (\text{E3})$$

This determines the intrinsic geometry. The second fundamental form is

$$\mathbf{II} = -d\mathbf{r} \cdot d\hat{\mathbf{n}}|_{\psi=\psi_0} = \kappa dl^2 - 2\rho\tau dl d\alpha - \rho \frac{\rho_{ll} - \rho\tau^2}{\kappa} d\alpha^2, \quad (\text{E4})$$

which controls the extrinsic geometry. By the Gauss-Bonnet theorem (see, e.g., Carmo 1976), the surface integral of the Gaussian curvature of a compact surface is equal to  $2\pi\chi$ , where  $\chi$  is the Euler characteristic of the surface. For the case of a toroidal surface,  $\chi = 0$ , so

$$0 = \int dA K = - \iint dl d\alpha \rho_{ll}. \quad (\text{E5})$$

For a QP surface, the Gauss-Bonnet theorem is an alternative expression of results that are already well known. The surface can be represented by a square grid in  $(l, \alpha)$ , since  $\alpha$  can be scaled to be an angle-like quantity in the range  $(0, 2\pi)$  and  $l$  is in the range  $(0, L)$  for  $L$  independent of  $\alpha$ —this is a documented property of quasisymmetry (see, e.g., Helander 2014 or §4). Then, noting that  $\rho$  is a single-valued quantity on the surface, the Gauss-Bonnet result (E5) is trivial.

The quasisymmetry vector  $\mathbf{u} = \partial_\alpha \mathbf{r}$  solves the Jacobi equation (see, e.g., Carmo 1976)

$$\frac{D^2 \mathbf{u}}{dl^2} + K (\hat{\mathbf{t}} \times \mathbf{u}) \times \hat{\mathbf{t}} = 0, \quad (\text{E6})$$

where we have defined the covariant derivative

$$\frac{D}{dl} = \hat{\mathbf{t}} \cdot \nabla \mathbf{v} - \hat{\mathbf{n}} \hat{\mathbf{n}} \cdot (\hat{\mathbf{t}} \cdot \nabla \mathbf{v}), \quad (\text{E7})$$

where  $\mathbf{v}$  is some vector in the surface's tangent plane. A foundational result of differential geometry is that the covariant derivative can be determined from the surface metric alone, through the Levi-Civita connection (Christoffel 1869; Levi-Civita 1916).

## Appendix F. Generalised helicoids as solutions to the surface equations

This appendix proves that generalised helicoids are the class of solutions to the surface equations when  $\rho_\alpha = \kappa_\alpha = \tau_\alpha = 0$ . We also show how the generalised helicoid, along with surfaces of revolution and surfaces generated by a planar curve translated in the binormal direction, are consequently the only cases where  $\mathbf{u}$  is a Killing vector of Euclidean space, i.e., the generator of helical, rotational, or translational motion.

Generalised helicoids can be parameterised by

$$\mathbf{r}(u, b) = (u \cos b, u \sin b, f(u) + ab) \quad (\text{F1})$$

for arbitrary smooth function  $f$  and constant  $a$  (Eisenhart 2013). This will be our starting point.

Thus, we have

$$\frac{\partial \mathbf{r}}{\partial u} = (\cos b, \sin b, f'(u)), \quad (\text{F2a})$$

$$\frac{\partial \mathbf{r}}{\partial b} = (-u \sin b, u \cos b, a), \quad (\text{F2b})$$

which gives the surface metric, also known as the first fundamental form,

$$I = (1 + f'(u)^2) du^2 + 2af'(u)dudb + (u^2 + a^2) db^2. \quad (\text{F3})$$

Compare this to the expression of the first fundamental form in  $(l, \alpha)$  coordinates, equation (E3). As well as being lines of inertial motion, geodesics are lines of shortest distance. So, the surface metric can be used to define an action from which we can apply the Lagrangian approach. In the Lagrangian sense,  $b$  is an ignorable coordinate. Given that we parameterise the geodesic in terms of arc length, the geodesic is determined by the conservation laws,

$$1 = (1 + f'(u)^2) \dot{u}^2 + 2af'(u)\dot{u}\dot{b} + (u^2 + a^2) \dot{b}^2, \quad (\text{F4a})$$

$$J = af'(u)\dot{u} + (u^2 + a^2)\dot{b}, \quad (\text{F4b})$$

where  $J$  is a constant of integration and the dot denotes a derivative with respect to  $l$ , the arc length along the geodesic.

The helices on the helicoid are given by  $u = \text{const}$ . In order for geodesics to be orthogonal to them, we take  $J = 0$ . Then, using equation (F4b), we can define the coordinate

$$\alpha = \int du \frac{af'(u)}{u^2 + a^2} + b, \quad (\text{F5})$$

as is also defined in Eisenhart (2013). Thus, we have

$$I = \left( 1 + \frac{u^2 f'(u)^2}{u^2 + a^2} \right) du^2 + (u^2 + a^2) d\alpha^2. \quad (\text{F6})$$

We can then define the arc length as

$$l = \int du \sqrt{1 + \frac{u^2 f'(u)^2}{u^2 + a^2}} \quad (\text{F 7})$$

to get

$$I = dl^2 + \rho^2 d\alpha^2, \quad (\text{F 8})$$

where  $\rho = \sqrt{u^2 + a^2}$  is independent of  $\alpha$ , as required.

We now show that  $\kappa$  and  $\tau$  are independent of  $\alpha$ . There is a direct method: find  $\dot{u}$  and  $\dot{b}$  from equations (F 4), calculate  $\hat{\mathbf{t}} = \dot{u}(\partial \mathbf{r}/\partial u)_b + \dot{b}(\partial \mathbf{r}/\partial b)_u$ , and calculate  $\kappa$  and  $\tau$  using the Frenet-Serret formulae. A quicker method uses the fact that the curvature  $\kappa$  and torsion  $\tau$  of a curve determine that curve uniquely, up to overall position and orientation ('the fundamental theorem of curves'). We therefore need only show that

$$\left( \frac{\partial \hat{\mathbf{t}}}{\partial \alpha} \right)_l = \mathbf{v}(\alpha) \times \hat{\mathbf{t}}, \quad (\text{F 9})$$

for some  $\mathbf{v}(\alpha)$  that is independent of  $l$ . Using the geodesic equations (F 4) we find

$$\hat{\mathbf{t}} = \frac{1}{\sqrt{1 + \frac{u^2 f'(u)^2}{u^2 + a^2}}} \begin{pmatrix} \cos b + \frac{au f'(u)}{u^2 + a^2} \sin b \\ \sin b - \frac{au f'(u)}{u^2 + a^2} \cos b \\ \frac{u^2 f'(u)}{u^2 + a^2} \end{pmatrix}. \quad (\text{F 10})$$

Then, noting that  $(\partial/\partial \alpha)_l = (\partial/\partial b)_u$ , we have equation (F 9) with  $\mathbf{v} = (0, 0, 1)$ . This completes the proof showing that  $\kappa$  and  $\tau$  are independent of  $\alpha$ .

We note that we have not explicitly shown that any solution where  $\rho_\alpha = \kappa_\alpha = \tau_\alpha = 0$  is a generalised helicoid. For this, we observe the fact that there is a helicoid corresponding to an arbitrary choice of  $\rho, \kappa$ , and  $\tau$  as functions of  $l$  (provided they obey the Codazzi-Mainardi equations) and that the Bonnet theorem applies.

We now show why generalised helicoids, and their limiting cases, are the only solutions to the surface equations where  $\mathbf{u}$  is a Killing vector of Euclidean space. To show this, we argue the stronger case that such surfaces are the only ones where  $\mathbf{u}$ , along a particular field line, can be extended to a Killing vector of Euclidean space. We reproduce a theorem from [Langer & Singer \(1984\)](#): a vector field  $\mathbf{u}$  along a field line extends to a Killing vector in Euclidean space if and only if  $\mathbf{u}$  satisfies

$$0 = \hat{\mathbf{t}} \cdot \frac{d\mathbf{u}}{dl}, \quad (\text{F 11a})$$

$$0 = \hat{\mathbf{n}} \cdot \frac{d^2\mathbf{u}}{dl^2}, \quad (\text{F 11b})$$

$$0 = \hat{\mathbf{b}} \cdot \left( \frac{d^3\mathbf{u}}{dl^3} - \frac{\kappa_l}{\kappa} \frac{d^2\mathbf{u}}{dl^2} + \kappa^2 \frac{d\mathbf{u}}{dl} \right), \quad (\text{F 11c})$$

where  $d/dl = \hat{\mathbf{t}} \cdot \nabla$ . By simple application of the Frenet-Serret formulae and the surface equations, these conditions are satisfied if and only if  $\rho_\alpha = \kappa_\alpha = \tau_\alpha = 0$ . The Killing vectors of Euclidean space are either generators of translations, rotations, or helical motion. For translations, we get surfaces of the form  $z = f(x)$ , where  $\hat{\mathbf{y}}$  is perpendicular to the field lines. For rotations, we get surfaces of revolution. For helical motion, we have generalised helicoids.

## Appendix G. QP objective functions for numerical optimisation

For the first set of configurations (1–3), which were produced in DESC, the QP objective function was

$$\frac{\int_0^{2\pi} d\vartheta \int_0^{2\pi} d\varphi \sqrt{g_{\text{surf}}} |\mathbf{B} \times \nabla B \cdot \nabla \psi|}{\int_0^{2\pi} d\vartheta \int_0^{2\pi} d\varphi \sqrt{g_{\text{surf}}} B^3}, \quad (\text{G } 1)$$

where  $\sqrt{g_{\text{surf}}} = |\partial_\theta \mathbf{r} \times \partial_\phi \mathbf{r}|$  is the Jacobian on the surface and  $2\pi\psi$  is the toroidal magnetic flux. The expression (G 1) is the two-term error used in Dudit *et al.* (2023).

For the second set of configurations (4–5), which were produced in SPEC and optimised for using the adjoint methods in Nies *et al.* (2022), the QP objective function was

$$\int_0^{2\pi} d\vartheta \int_0^{2\pi} d\varphi \sqrt{g_{\text{surf}}} \left( \frac{1}{B^3} \mathbf{B} \times \nabla B \cdot \nabla \psi \right)^2. \quad (\text{G } 2)$$

Because there are not necessarily nested flux surfaces within the boundary, defining  $\nabla\psi$  in this case is a subtle issue that is dealt with in Nies *et al.* (2022).

## Appendix H. Numerical calculation of $\rho$

In this appendix, we show that the numerical calculation of  $\rho$  as per equation (5.4) agrees with the theoretical definition used in this paper.

The surface Jacobian  $J$  in  $(l, \alpha)$  coordinates is  $J^{(l, \alpha)} = \rho$ . Therefore, assuming a QP equilibrium, the surface Jacobian in Boozer coordinates is

$$J^{(\theta, \phi)} = \frac{G}{B} \rho, \quad (\text{H } 1)$$

where we have used the transformation ( $l = l(\theta, \phi), \alpha = \alpha(\theta, \phi)$ ) given in appendix C. Furthermore, using the standard transformation between Boozer coordinates and computational coordinates  $(\vartheta, \varphi)$  given by equations (5.3), we transform the surface Jacobian

$$\sqrt{g_{\text{surf}}} := J^{(\vartheta, \varphi)} = \left| (1 + \omega_\phi)(1 + \tilde{\lambda}_\theta) - \omega_\theta(\tilde{\lambda}_\phi - \iota) \right| J^{(\theta, \phi)}. \quad (\text{H } 2)$$

Combining equations (H 1) and (H 2) gives equation (5.4).

## Appendix I. LQP surfaces that are perturbations to magnetic mirrors

In this appendix, we provide a mathematical argument based on the surface equations for why numerical QP equilibria tend to have narrow pinch points and high mirror ratios. This calculation is based on the identification of QP equilibria with ‘linked magnetic mirrors’. The calculation considers small perturbations to magnetic mirrors through the surface equations. We use this approach to derive the properties of the mirror-like surface that most readily permit the surface to ‘bend around’ (as is necessary to form a toroidal surface) and generate a non-zero rotational transform. The schematic idea of perturbing a magnetic mirror is shown in figure 11. We now proceed through this calculation.

As the zeroth-order equilibrium surface solution, we take a surface of revolution with meridians as field lines:

$$\mathbf{r}(l, \alpha) = (x(l), y(l) \cos \alpha, y(l) \sin \alpha), \quad (\text{I } 1)$$

where  $l$  is the arc length of the field lines, so  $x'^2 + y'^2 = 1$ . We use primes to signify a derivative with respect to  $l$ . For such a surface, the field lines have zero torsion (since they are planar), the (signed) curvature is  $\kappa_0 = y''/x'$ , and we also have  $\rho_0 = y$ . We also

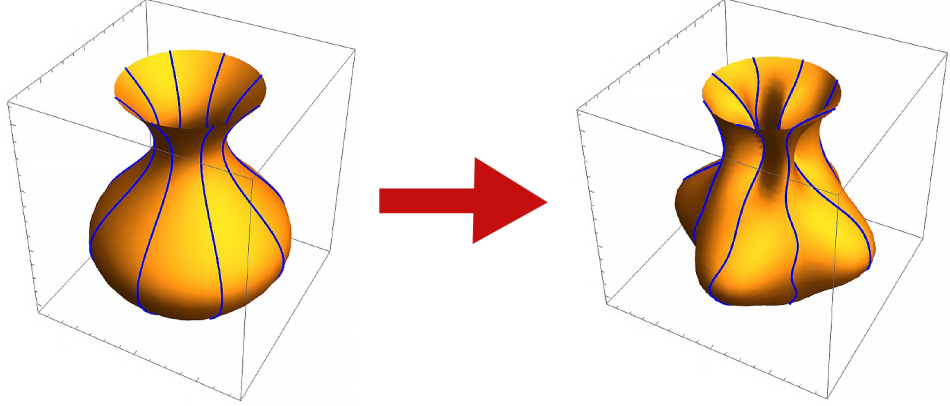


FIGURE 11. An illustrative picture of the perturbation to a magnetic mirror.

define  $\gamma := \kappa_0/\rho_0$ . Defined in this way, the surface normal points inwards and  $\alpha$  is an angle-like coordinate in the range  $[0, 2\pi)$ .

We now consider small perturbations to the equilibrium magnetic-mirror solution,

$$\rho = \rho_0 + \delta\rho, \quad (I2a)$$

$$\kappa = \kappa_0 + \delta\kappa, \quad (I2b)$$

$$\tau = \delta\tau. \quad (I2c)$$

Since we work with linear equations with coefficients that are independent of  $\alpha$ , it is useful to expand in Fourier modes of  $\alpha$ ,

$$\delta\rho = \sum_{m=-\infty}^{\infty} \delta\rho_m(l) e^{im\alpha}, \quad (I3)$$

and similarly for  $\delta\kappa$  and  $\delta\tau$ . We note that  $m$  is restricted to integers, since  $\alpha$  is an angle-like coordinate. For non-trivial results, we focus on the case where the perturbations are  $\alpha$ -dependent, so we ignore the  $m = 0$  mode. The  $m = \pm 1$  modes are particularly relevant for a toroidal geometry, since a positive  $\delta\kappa$  on one side of the surface and a negative  $\delta\kappa$  on the opposing side would lead to the surface ‘bending around’. This is akin to the Ackermann steering geometry for a turning car, where one wheel turns more than another. Additionally, non-zero  $\delta\tau$  can be interpreted as the generator of a non-zero rotational transform  $\iota$ .

Linearising the third surface equation (3.8c) leads to  $\delta\kappa_m = \gamma\delta\rho_m$ . Substituting for  $\delta\kappa_m$  in the other surface equations gives

$$im\gamma\delta\rho_m = -\frac{(\rho_0^2\delta\tau_m)'}{\rho_0}, \quad (I4a)$$

$$im\delta\tau_m = \gamma(\rho_0\delta\rho)' + \left( \frac{1}{\gamma\rho_0} \left( \delta\rho_m'' - \frac{\rho_0''}{\rho_0} \delta\rho_m \right) \right)'. \quad (I4b)$$

These two equations are equivalent to a fourth-order ODE in  $l$ , with  $m$  as a parameter.

For tractability, we simplify this system by taking  $\gamma \rightarrow \infty$  whilst holding  $\gamma\delta\rho_m = \delta\kappa_m$  fixed. In this case, the second set of terms on the right-hand side of equation (I4b) can be neglected, reducing the order of the differential equation system from four to two. This limit corresponds to a magnetic mirror with large axisymmetric curvature  $\kappa_0$ . Then, the

system of linearised equations is equivalent to

$$\frac{1}{\gamma} (\gamma \rho_0^2 \xi'_m)' = m^2 \xi_m, \quad (I5)$$

where  $\xi_m = \rho_0 \delta \rho_m$  and  $\delta \tau_m = -\frac{i}{m} \gamma \xi'_m$ . Due to the fact that a stellarator surface closes up on itself, often with a further field-period symmetry, it is natural to consider a periodic surface of revolution and consider periodic perturbations. We take  $L$  to be the distance along a field line across one period of the surface of revolution. With such boundary conditions, there exist two infinite, unbounded sequences of real eigenvalues  $\{\lambda_{+n}\}$  and  $\{\lambda_{-n}\}$  such that

$$0 < \lambda_{+1} < \lambda_{+2} < \dots \rightarrow \infty, \quad (I6a)$$

$$0 > \lambda_{-1} > \lambda_{-2} > \dots \rightarrow -\infty, \quad (I6b)$$

([Haupt 1915](#); [Richardson 1918](#); [Atkinson & Mingarelli 1987](#); [Constantin 1997](#)). The square of an integer is, in general, not in the spectrum for any particular surface of revolution, recalling that the  $\lambda = m^2 = 1$  case is the most relevant for toroidal geometries. Therefore, the surface needs to be finely tuned to admit perturbations.

Now, we are positioned to understand why narrow pinch points arise in the observed configurations. We note the result of [Atkinson & Mingarelli \(1987\)](#), which states that the asymptotic form for  $\lambda_{+n}$  as  $n \rightarrow \infty$  is

$$\lambda_{+n} \sim \frac{n^2 \pi^2}{\left( \int_0^L \frac{dl}{y} \right)^2}. \quad (I7)$$

Thus, the density of positive eigenvalues increases, in the asymptotic limit, if  $y$  has a small minimum (i.e., the surface of revolution has a narrow pinch point). Notably, due to the term  $1/y$  in the integrand of the denominator, a pinch point has a seemingly larger effect than scaling down the cross-sectional area of the magnetic mirror or increasing  $L$ . Thus, given a higher density of eigenvalues, we claim that smaller fine-tuned adjustments of the magnetic mirror are required to produce a perturbation with  $\lambda = 1$ . Thus, *it is ‘easier’ for a magnetic mirror with a narrower pinch point to ‘bend around’ whilst remaining an LQP surface*. Similarly, it is ‘easier’ for a magnetic mirror with a narrower pinch point to have a non-zero rotational transform. In a toroidal equilibrium, narrow pinch points are also associated with larger magnetic field strengths, since field lines are compressed together. This leads to the observed high mirror ratios.

We caution that this argument is not rigorous as we employed several simplifying assumptions. Firstly, we neglected terms corresponding to finite  $\kappa_0$  to reduce the order from four to two. Secondly, we assumed that the eigenvalues can be shifted slightly by small deformations of the magnetic mirror. This allowed us to conclude from an increased density of eigenvalues that it is ‘easier’ for a magnetic mirror with a pinch point to have a  $\lambda = 1$  eigenvalue. Thirdly, we assumed that a higher density of eigenvalues in the asymptotic limit of  $n \rightarrow \infty$  also relates to a higher density of eigenvalues around  $\lambda = 1$ .

## REFERENCES

ALCUSON, J.A., REYNOLDS-BARREDO, J.M., BUSTOS, A., SANCHEZ, R., TRIBALDOS, V., XANTHOPOULOS, P., GOERLER, T. & NEWMAN, D.E. 2016 Quasi-symmetry and the nature of radial turbulent transport in quasi-poloidal stellarators. *Physics of Plasmas* **23** (10), 102308.

ATKINSON, F.V. & MINGARELLI, A.B. 1987 Asymptotics of the number of zeros and of

the eigenvalues of general weighted Sturm-Liouville problems. *Journal für die reine und angewandte Mathematik* **0375** – **0376**, 380–393.

BATCHELOR, G.K. 1967 *An Introduction to Fluid Dynamics*. Cambridge University Press.

BETCHOV, R. 1965 On the curvature and torsion of an isolated vortex filament. *Journal of Fluid Mechanics* **22** (3), 471–479.

BISWAS, A., MILOVIC, D. & EDWARDS, M. 2010 *Nonlinear Schrödinger's Equation*, pp. 5–26. Berlin, Heidelberg: Springer Berlin Heidelberg.

BOOZER, A.H. 1981 Plasma equilibrium with rational magnetic surfaces. *The Physics of Fluids* **24** (11), 1999–2003.

BOOZER, A.H. 1995 Quasi-helical symmetry in stellarators. *Plasma Physics and Controlled Fusion* **37** (11A), A103.

CAMACHO MATA, K., PLUNK, G.G. & JORGE, R. 2022 Direct construction of stellarator-symmetric quasi-isodynamic magnetic configurations. *Journal of Plasma Physics* **88** (5), 905880503.

CARMO, M.P.D. 1976 *Differential geometry of curves and surfaces*. Englewood Cliffs, N.J.: Prentice-Hall.

CARTAN, E. 2001 *Riemannian geometry in an orthogonal frame : from lectures delivered by Élie Cartan at the Sorbonne in 1926-1927*. River Edge, NJ: World Scientific.

CHRISTOFFEL, E.B. 1869 Ueber die transformation der homogenen differentialausdrücke zweiten grades. *Journal für die reine und angewandte Mathematik* **1869** (70), 46–70.

CLEBSCH, A. 1859 Ueber die integration der hydrodynamischen gleichungen. *Journal für die reine und angewandte Mathematik* **1859** (56), 1–10.

CODAZZI, D. 1868 Sulle coordinate curvilinee d'una superficie e dello spazio. *Annali di Matematica Pura ed Applicata (1867-1897)* **2** (1), 101–119.

CONSTANTIN, A. 1997 A general-weighted Sturm-Liouville problem. *Annali della Scuola Normale Superiore di Pisa - Classe di Scienze* **24** (4), 767–782.

DA RIOS, L.S. 1906 Sul moto d'un liquido indefinito con un filetto vorticoso di forma qualunque. *Rendiconti del Circolo Matematico di Palermo (1884-1940)* **22** (1), 117–135.

DARBOUX, G. 2000 *Lecons Sur la Theorie Generale Des Surfaces Et Les Applications Geometriques Du Calcul Infinitesimal: Four-Volume Set*. American Mathematical Society.

DEPMAN, I.Y. 1952 Karl mikhailovich peterson i ego kandidatskaya dissertatsia [karl m. peterson and his candidate's dissertation]. *Istoriko-matematicheskie issledovaniya* **5**.

DUDT, D.W., CONLIN, R., PANICI, D. & KOLEMEN, E. 2023 The desc stellarator code suite part 3: Quasi-symmetry optimization. *Journal of Plasma Physics* **89** (2), 955890201.

DUDT, D.W. & KOLEMEN, E. 2020 Desc: A stellarator equilibrium solver. *Physics of Plasmas* **27** (10), 102513.

EISENHART, L.P. 2013 *A Treatise on the Differential Geometry of Curves and Surfaces*. Dover Books on Mathematics . Dover Publications.

FRENET, F. 1852 Sur les courbes à double courbure. *Journal de Mathématiques Pures et Appliquées* pp. 437–447.

FROBENIUS, G. 1877 Ueber das pfaffsche problem. *Journal für die reine und angewandte Mathematik* **1877** (82), 230–315.

GARDNER, C.S., GREENE, J.M., KRUSKAL, M.D. & MIURA, R.M. 1967 Method for solving the Korteweg-De Vries equation. *Phys. Rev. Lett.* **19**, 1095–1097.

GARREN, D.A. & BOOZER, A.H. 1991 Existence of quasihelically symmetric stellarators. *Physics of Fluids B: Plasma Physics* **3** (10), 2822–2834.

GAUSS, C.F. 1828 Disquisitiones generales circa superficies curvas [general discussions about curved surfaces]. *Comm. Soc. Gott.* **6**.

GOODMAN, A.G., CAMACHO MATA, K., HENNEBERG, S.A., JORGE, R., LANDREMAN, M., PLUNK, G.G., SMITH, H.M., MACKENBACH, R.J.J., BEIDLER, C.D. & HELANDER, P. 2023 Constructing precisely quasi-isodynamic magnetic fields. *Journal of Plasma Physics* **89** (5), 905890504.

HALL, L.S. & McNAMARA, B. 1975 Three-dimensional equilibrium of the anisotropic, finite-pressure guiding-center plasma: Theory of the magnetic plasma. *The Physics of Fluids* **18** (5), 552–565.

HAQUE, M., PAUL, E.J., GIULIANI, A., CAMPAGNA, M., MADAN, R. & SENGUPTA, W. 2026 Optimization for quasi-poloidal symmetry. *Forthcoming*.

HASIMOTO, H. 1972 A soliton on a vortex filament. *Journal of Fluid Mechanics* **51** (3), 477–485.

HAUPT, O. 1915 Über eine methode zum beweise von oszillationstheoremen. *Mathematische Annalen* **76**, 67–104.

HEGNA, C.C. ET AL. 2025 The Infinity Two fusion pilot plant baseline plasma physics design. *Journal of Plasma Physics* **91** (3), E76.

HELANDER, P. 2014 Theory of plasma confinement in non-axisymmetric magnetic fields. *Reports on Progress in Physics* **77** (8), 087001.

HELANDER, P. ET AL. 2012 Stellarator and tokamak plasmas: a comparison. *Plasma Physics and Controlled Fusion* **54** (12), 124009.

HIRSHMAN, S.P. & WHITSON, J.C. 1983 Steepest-descent moment method for three-dimensional magnetohydrodynamic equilibria. *The Physics of Fluids* **26** (12), 3553–3568.

HUDSON, S.R., DEWAR, R.L., DENNIS, G., HOLE, M.J., MCGANN, M., VON NESSI, G. & LAZERSON, S. 2012 Computation of multi-region relaxed magnetohydrodynamic equilibria. *Physics of Plasmas* **19** (11), 112502.

IMBERT-GERARD, L., PAUL, E.J. & WRIGHT, A.M. 2024 *An introduction to stellarators: From magnetic fields to symmetries and optimization*. SIAM.

JORGE, R., PLUNK, G.G., DREVLAK, M., LANDREMAN, M., LOBSIEN, J.-F., CAMACHO MATA, K. & HELANDER, P. 2022 A single-field-period quasi-isodynamic stellarator. *Journal of Plasma Physics* **88** (5), 175880504.

KIDA, S. 1981 A vortex filament moving without change of form. *Journal of Fluid Mechanics* **112**, 397.

LAKSHMANAN, M. 1977 Continuum spin system as an exactly solvable dynamical system. *Physics Letters A* **61** (1), 53–54.

LANDREMAN, M. 2011 Electric fields and transport in optimized stellarators. Ph.D. thesis, Massachusetts Institute of Technology, Cambridge, MA.

LANDREMAN, M. & PAUL, E. 2022 Magnetic fields with precise quasisymmetry for plasma confinement. *Phys. Rev. Lett.* **128**, 035001.

LANDREMAN, M. & SENGUPTA, W. 2019 Constructing stellarators with quasisymmetry to high order. *Journal of Plasma Physics* **85** (6), 815850601.

LANGER, J. & SINGER, D. 1984 Knotted elastic curves in R3. *Journal of the London Mathematical Society* **s2-30**.

LEVI-CIVITA, MEMORIA DI T. 1916 Nozione di parallelismo in una varietà qualunque e conseguente specificazione geometrica della curvatura riemanniana. *Rendiconti del Circolo Matematico di Palermo (1884-1940)* **42** (1), 173–204.

LION, J. ET AL. 2025 Stellaris: A high-field quasi-isodynamic stellarator for a prototypical fusion power plant. *Fusion Engineering and Design* **214**, 114868.

MAINARDI, G. 1856 Su la teoria generale delle superficie. *Giornale Dell' Istituto Lombardo* **9**, 385–404.

MERCIER, C. 1964 Equilibrium and stability of a toroidal magnetohydrodynamic system in the neighbourhood of a magnetic axis. *Nuclear Fusion* **4** (3), 213.

NELSON, B.E. ET AL. 2003 Design of the quasi-poloidal stellarator experiment (QPS). *Fusion Engineering and Design* **66-68**, 205–210, 22nd Symposium on Fusion Technology.

NIES, R., PAUL, E.J., HUDSON, S.R. & BHATTACHARJEE, A. 2022 Adjoint methods for quasisymmetry of vacuum fields on a surface. *Journal of Plasma Physics* **88** (1), 905880106.

NÜHRENBERG, J. & ZILLE, R. 1988 Quasi-helically symmetric toroidal stellarators. *Physics Letters A* **129** (2), 113–117.

ORAEVSKII, V.N. 1962 Stability of ionic longitudinal oscillations of plasma in magnetic field. *Zh. Prikl. Mekhan. I Tekhn. Fiz.* **5**.

PALUMBO, D. 1968 Some considerations on closed configurations of magnetohydrostatic equilibrium. *Il Nuovo Cimento B (1965-1970)* **53** (2), 507–511.

RICHARDSON, R.G.D. 1918 Contributions to the study of oscillation properties of the solutions of linear differential equations of the second order. *American Journal of Mathematics* **40** (3), 283–316.

RIEMANN, B. & WEBER, H. 1953 *The Collected Works of Bernhard Riemann*. Dover Publications.

RODRIGUEZ, E. 2022 Quasisymmetry. PhD thesis, Princeton University, Princeton, NJ.

RODRÍGUEZ, E., HELANDER, P. & BHATTACHARJEE, A. 2020 Necessary and sufficient conditions for quasisymmetry. *Physics of Plasmas* **27** (6), 062501.

RODRÍGUEZ, E., SENGUPTA, W. & BHATTACHARJEE, A. 2021 Generalized boozer coordinates: A natural coordinate system for quasisymmetry. *Physics of Plasmas* **28** (9), 092510.

RODRÍGUEZ, E., SENGUPTA, W. & BHATTACHARJEE, A. 2023 Constructing the space of quasisymmetric stellarators through near-axis expansion. *Plasma Physics and Controlled Fusion* **65** (9), 095004.

ROGERS, C. & SCHIEF, W.K. 2002 *Bäcklund and Darboux Transformations: Geometry and Modern Applications in Soliton Theory*. Cambridge University Press.

SCHIEF, W.K. 2003 Nested toroidal flux surfaces in magnetohydrostatics. generation via soliton theory. *Journal of Plasma Physics* **69** (6), 465–484.

SENGUPTA, W., NIKULSIN, N., BULLER, S., MADAN, R., PAUL, E.J., NIES, R., KAPTANOGLU, A.A., HUDSON, S.R. & BHATTACHARJEE, A. 2024 Periodic korteweg-de vries soliton potentials generate magnetic field strength with excellent quasisymmetry.

SERRET, J.A. 1851 Sur quelques formules relatives à la théorie des courbes à double courbure. *Journal de Mathématiques Pures et Appliquées* pp. 193–207.

SHAFRANOV, V.D. 1963 Equilibrium of a toroidal pinch in a magnetic field. *Soviet Atomic Energy* **13** (6), 1149–1158.

SHAING, K.C. & CALLEN, J.D. 1983 Neoclassical flows and transport in nonaxisymmetric toroidal plasmas. *The Physics of Fluids* **26** (11), 3315–3326.

SPITZER, L.J. 1958 The Stellarator Concept. *The Physics of Fluids* **1** (4), 253–264.

SPOONG, D.A., HIRSHMAN, S.P., LYON, J.F., BERRY, L.A. & STRICKLER, D.J. 2005 Recent advances in quasi-poloidal stellarator physics issues. *Nuclear Fusion* **45** (8), 918.

SÁNCHEZ, E., VELASCO, J.L., CALVO, I. & MULAS, S. 2023 A quasi-isodynamic configuration with good confinement of fast ions at low plasma  $\beta$ . *Nuclear Fusion* **63** (6), 066037.

TERRY, P.W. 2000 Suppression of turbulence and transport by sheared flow. *Rev. Mod. Phys.* **72**, 109–165.

VELASCO, J.L., CALVO, I., SÁNCHEZ, E. & PARRA, F.I. 2023 Robust stellarator optimization via flat mirror magnetic fields. *Nuclear Fusion* **63** (12), 126038.

WARE, A.S., WESTERLY, D., BARCIKOWSKI, E., BERRY, L.A., FU, G.Y., HIRSHMAN, S.P., LYON, J.F., SÁNCHEZ, R., SPOONG, D.A. & STRICKLER, D.J. 2004 Second ballooning stability in high- $\beta$ , compact stellarators. *Physics of Plasmas* **11** (5), 2453–2458.

WOBIG, H. 1999 Theory of advanced stellarators. *Plasma Physics and Controlled Fusion* **41** (3A), A159.

ZAKHAROV, V.E. 1968 Stability of periodic waves of finite amplitude on the surface of a deep fluid. *Journal of Applied Mechanics and Technical Physics* **9** (2), 190–194.